Dynamical interplay of disc shear and interstellar gas on the pitch angle of swing amplified spirals in galaxies

M.Sc. Thesis

by

SANGEETA



DEPARTMENT OF ASTRONOMY, ASTROPHYSICS & SPACE ENGINEERING

INDIAN INSTITUTE OF TECHNOLOGY INDORE

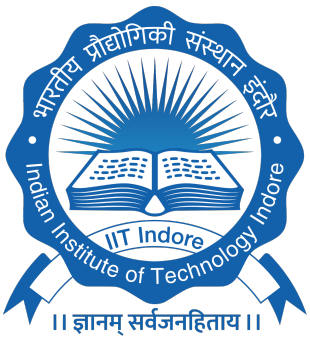
May, 2026

Dynamical interplay of disc shear and interstellar gas on pitch angle of swing amplified spirals in galaxies

A THESIS

Submitted in partial fulfillment of the requirements for the award of the degree
of
Master of Science

by
SANGEETA



DEPARTMENT OF ASTRONOMY, ASTROPHYSICS & SPACE ENGINEERING

INDIAN INSTITUTE OF TECHNOLOGY INDORE

ACKNOWLEDGEMENTS

There is something quietly strange about sitting down to write the acknowledgement section of my thesis it means the work is done, or at least done enough to be called a thesis and as I write this, I find myself pausing to think about how this journey began, what it has given me, and the people without whom none of it would have been possible.

First and foremost, I wish to express my deepest gratitude to my supervisor, Dr. Soumavo Ghosh, who introduced me to this beautiful and endlessly fascinating world of galactic dynamics and spiral structure. His patience in the face of my early confusions, his clarity in untangling complex ideas, and his genuine enthusiasm for the science were a constant source of motivation. Every discussion whether brief and pointed left me with something new to think about. For his guidance and time I am deeply and sincerely grateful.

Also I would like to acknowledge generous support from IIT-Indore through Dr. Soumavo Ghosh's YFRSG-Dream-PRIUS funding (IITI/YFRSG-Dream-PRIUS/Phase-I/2025-26/06). I would also like to thank the faculty of the Department of Astronomy, Astrophysics & Space Engineering at IIT Indore for providing an intellectually and welcoming environment. Their passion for teaching and research created a space where curiosity felt valued.

A sincere word of thanks, to my family who stood by me with unwavering love and belief, asking nothing in return except that I do my best. They never needed to understand every equation in this thesis to understand why it mattered to me, and that quiet faith has meant more than words can easily say. This work, in its small and honest way, belongs to them too.

I wish to convey my sincere thanks to my close friends, Amrita Yadav and Neha Verma, for their invaluable support and encouragement during the course of this research

And finally, thanks to my friends and fellow M.Sc classmates whose company made even the difficult days feel lighter. The problem-solving sessions, the shared frustrations over code that refused to run or having some confusion, and the small celebrations when it finally did — these are the things that make a research experience fun. I am glad to have been through this alongside you.

Sangeeta
2403121011
IIT Indore

DEDICATION

To my family, who stood beside me through every success and failure, and whose love has always been my greatest strength.

INDIAN INSTITUTE OF TECHNOLOGY INDORE

CANDIDATE'S DECLARATION

I hereby certify that the work which is being presented in the thesis entitled **DYNAMICAL INTERPLAY OF DISC SHEAR AND INTERSTELLAR GAS ON THE PITCH ANGLE OF SWING AMPLIFIED SPIRALS IN GALAXIES** in the partial fulfillment of the requirements for the award of the degree of **MASTER OF SCIENCE** and submitted in the **DEPARTMENT OF ASTRONOMY, ASTROPHYSICS and SPACE ENGINEERING, Indian Institute of Technology Indore**, is an authentic record of my own work carried out during the time period from June 2024 to May 2026 under the supervision of Dr. Soumavo Ghosh, Assistant Professor, Discipline of Astronomy, Astrophysics and Space Engineering (DAASE), Indian Institute of Technology Indore.

The matter presented in this thesis has not been submitted by me for the award of any other degree of this or any other institute.

Sangeeta

07.05.2026
Signature of the student with date
(SANGEETA)

This is to certify that the above statement made by the candidate is correct to the best of my/our knowledge.

Soumavo Ghosh.

07.05.2026
Signature of the Supervisor of

M.Sc. thesis (with date)

(Dr. SOUMAVO GHOSH)

SANGEETA has successfully given her M.Sc. Oral Examination held on **5 May, 2026.**

Soumavo Ghosh.

Signature(s) of Supervisor(s) of MSc thesis
Date:06.05.2026

Manoneeta Chakraborty

Programme Coordinator, M.Sc.
Date: 08/05/2026

Manoneeta Chakraborty

Convenor, DPGC
Date: 08/05/2026

S. Das

HoD, DAASE
Date: 08/05/2026

ABSTRACT

Spiral arms are one of the the most prominent non-axisymmetric structures in disc galaxies, and their morphology is strongly influenced different dynamical factors in the galactic disc. The pitch angle is one of the most fundamental morphological properties of spiral arms, as it directly quantifies the degree of winding of the spiral structure. However, which dynamical factors influence the variation of pitch angle – a full consensus is still largely missing.

In this work, we investigate the dependence of the pitch angle and strength (maximum amplification factor) of swing-amplified spiral arms on galactic disc shear rate with varying parameters, for example, disc scale height β, Toomre stability factor Q, gas mass fraction ϵ and X. The analysis begins with a one-fluid stellar galactic disc model in the infinitesimally thin limit and is subsequently extended to finite disc thickness. We further consider a more realistic two-fluid galactic disc composed of gravitationally coupled stars and interstellar gas. The calculations are carried out over a wide range of Toomre stability parameter Q, dimensionless wavelength parameter X, disc thickness parameter β (for the one-fluid case), thickness parameters $\beta_{\rm s}$ and $\beta_{\rm g}$ (for the two-fluid case), shear rate η, and gas mass fraction ϵ.

We find that the pitch angle decreases monotonically with increasing shear rate for all values of Q, X, and disc thickness β, indicating that stronger differential rotation produces more tightly wound spiral arms. In the one-fluid case, the pitch angle further decreases with increasing X, while finite disc thickness increases the pitch angle, producing relatively more open spiral structures. The maximum amplification factor decreases systematically with increasing disc thickness, with the suppression becoming stronger at larger Q. For the two-fluid case, the pitch angle decreases monotonically with increasing shear rate in both the stellar and gaseous components. Increasing the gas mass fraction ϵ produces relatively tighter spiral structures, particularly in the gaseous component, while increasing the stellar disc thickness leads to more open spiral arms in both components. Overall, the gaseous component remains more tightly wound than the stellar component. In conclusion, our study reveals a more comples variation of pitch angle in disc galaxies, depending strongly on shear rate, disc thickness and interstellar gas fraction.

TABLE OF CONTENTS

ACKNOWLEDGEMENTS **3**

DEDICATION **5**

ABSTRACT **7**

LIST OF FIGURES **11**

1 Introduction **1**
- 1.1 Occurrence of Spiral arm in real galaxies . . . 1
- 1.2 Multi-Wavelength appearance of Spiral arms in galaxies . . . 2
- 1.3 Properties of Spiral arm . . . 5
  - 1.3.1 Spiral arm multiplicity . . . 5
  - 1.3.2 Strength of Spiral arms . . . 5
  - 1.3.3 Pitch angle . . . 6
  - 1.3.4 The pitch angle vs shear relation and its discrepancies . . . 8
- 1.4 Density wave theory . . . 9
  - 1.4.1 Limitations of the density wave theory . . . 10
- 1.5 Swing Amplification . . . 11
  - 1.5.1 Effect of shear rate in swing amplification . . . 11
  - 1.5.2 Effect of epicyclic motion in swing amplification . . . 11
  - 1.5.3 Effect of self gravity on swing amplification . . . 12
  - 1.5.4 Effect of pressure on swing amplification . . . 13
- 1.6 Scientific Goal of my Work . . . 13

2 Formulation of swing amplification in disc galaxies **15**
- 2.1 One-fluid galactic disc with finite thickness . . . 15
  - 2.1.1 Numerical Solution . . . 20
- 2.2 Two-fluid galactic disc with finite thickness . . . 20

3 Results **27**
- 3.1 Variation of swing-amplified spirals with shear rate for One fluid case . 27
  - 3.1.1 Variation of MAF with shear rate . . . 27
  - 3.1.2 Variation of pitch angle with shear rate . . . 30
  - 3.1.3 Dependence of pitch angle variation with X . . . 34
  - 3.1.4 Variation of the pitch angle and shear rate with different values of X . . . 35
- 3.2 Comparsion with the past studies . . . 36
- 3.3 Variation of swing-amplifies spirals with shear rate for two fluid (stars+gas) case . . . 38

4 Conclusion & Future Plans **43**

LIST OF FIGURES

1.1 Examples of disc galaxies showing a wide range of spiral morphologies. This sample includes grand-design spirals such as NGC 5194 (M51) and NGC 1566, multi-armed and intermediate spirals like NGC 5054 and M 63, as well as galaxies with unusual or counter-winding spiral structures such as NGC 4622. *Image credits:* HST, PanSTARRS. 1

1.2 *One galaxy many faces:* the Milky Way viewed at ten different wavelength regimes from radio to gamma rays, illustrating how different spectral bands trace distinct physical component of galactic disc. In this map the central part of the galaxy in a band that extends up to 10° north and 10° south of the galactic plane (NASA Goddard Space Flight Center, 2010). 4

1.3 Examples of different spiral-arm multiplicity. (a) shows a grand-design spiral galaxy, Milky Way galaxy (b) illustrates a multi-arm spiral galaxy, and panel (c) represents a flocculent spiral galaxy, revealing the wide range of structures observed in spiral systems across the local universe. *Image credits:* HST, NASA/JPL-Caltech. 6

1.4 Pitch angle γ of a spiral arm. The pitch angle is defined as the angle between the tangent to the spiral (red curve) and concentric circle around galactic center (blue circle). 6

1.5 Schematic representation of the Hubble tuning fork diagram showing the morphological classification of galaxies. The sequence begins with elliptical galaxies ranging from E0 to E7, followed by lenticular galaxies (S0) at the junction point. From S0, the sequence bifurcates into normal spiral galaxies (Sa, Sb, Sc) and barred spiral galaxies (SBa, SBb, SBc). Along both spiral branches, the bulge size decreases and the spiral arms become more open and loosely wound from early-type to late-type galaxies *Image credits:* NASA and ESA 8

1.6 Spiral arms as density waves. The pattern remains stable over time despite differential rotation, analogous to a traffic jam where individual cars move through but the congestion persists (Image: Wikipedia). . . . 9

2.1 Evolution of θ, the ratio of the perturbed to unperturbed surface density, as a function of the dimensionless time τ in the sheared frame. The perturbation begins in a leading configuration ($\tau < 0$) and is transformed into a trailing one ($\tau > 0$) by the differential rotation of the disc. The point $\tau \approx 0$ corresponds to the leading-to-trailing transition, during which swing amplification reaches at its maximum value. 18

2.2 Evolution of θ, the ratio of the perturbed to unperturbed surface density, as a function of the dimensionless time (τ), in the sheared frame with different galactic disc height β (0.0, 0.1, 0.2, 0.3, 0.4, 0.5) for Toomre stability factor $Q = 1.3$, $X = 1$, $\eta = 1$, respectively. The maximum amplification factor (MAF) decreases with an increase in the disc thickness. 19

2.3 Evolution of θ, the ratio of the perturbed to unperturbed surface density, as a function of the dimensionless time (τ), for the stellar and gaseous components in a two-fluid galactic disc. The black curve corresponds to the stellar component with $Q_s = 1.8$ and $\beta_s = 0.5$, while the orange curve represents the gaseous component with $Q_g = 1.2$ and $\beta_g = 0.1$. . 24

3.1 The temporal evolution of $\theta = \delta\Sigma/\Sigma$, the ratio of the perturbed to unperturbed surface density, as a function of the dimensionless time (τ), in the sheared frame with different shear rate (η) (see the colour bar) with parameter fixed at $Q = 1.1$, $\beta = 0.1$, $X = 1$. 27

3.2 Systematic variation of the Maximum Amplification Factor (MAF) with the shear rate (η) for swing amplified spiral arms, for different disc scale height (β) and for different values of Toomre Q parameter. For given Q value, and for a fixed β, the MAF tends to attain its maximum around $\eta \sim 1$. This trend holds true for almost the entire parameter regime considered here. 28

3.3 Systematic variation of the pitch angle (γ) with the shear rate (η) for swing amplified spiral arms, for different disc scale height (β) and for different value of Toomre Q parameter at wavelength parameter X = 1. 30

3.4 Pitch angle (γ) as a function of the shear rate η for $Q = 1.1$, $\beta = 0.1$, and $X = 1.0$. The blue markers denote the numerical results obtained from the swing amplification calculations. The solid orange curve represents the best exponential fit to the data, $\gamma = A\exp(-B(\eta - \eta_0)$, where the η_0 is 0.4, with the fitted parameters $A = 30.5929 \pm 0.5303$ and $B = 0.6883 \pm 0.029$. 31

3.5 *Quantifying the fall-off of the pitch angle with the shear*: the exponential decay rate of the pitch angle with shear, shown for different Toomre Q parameters. For details, see the text. 33

3.6 Systematic variation of the pitch angle (γ) with the shear rate (η) for swing amplified spiral arms, for different disc scale height (β) and for different value of Toomre Q parameter with different value wavelength parameter 1.5 and 2.0 34

3.7 *Quantifying the fall-off of the pitch angle with the shear*: the exponential decay rate of the pitch angle with shear, shown for different Toomre Q parameterswith different X values. 35

3.8 Comparison with previous studies: The variation of the pitch angle (γ) with shear rate (η) is shown for different values of the Toomre parameter Q (see columns) and the wavelength parameter X (see rows). The coloured points represent the present calculations from swing amplification for different values of the disc scale height (β), (see the colour bar). The dashed black and grey lines correspond to the best fit results from previous studies Michikoshi and Kokubo (2014) and Marc S. Seigar et al. (2006) respectively. The shaded region represents the observational relation reported in (Marc S. Seigar et al., 2006) 36

3.9 Variation of pitch angle (γ) with shear rate (η) for different values of the gas mass fraction (ϵ). The top row corresponds to the stellar component, while the bottom row represents the gaseous component. Each panel shows results for a fixed β_s. Different colored curves denote different values gas mass fraction ϵ, (see the colour bar) while the gas scale height is kept fixed ($\beta_g = 0.1$). In all cases, the pitch angle decreases with increasing shear rate, indicating more tightly wound spiral structures at higher differential rotation. 39
3.10 The exponential decay of pitch angle with shear rate for two fluid case, shown for different value of gas mass fraction (ϵ), with different value of disc scale height and Toomre factor ($Q_s = 2.0, Q_g = 2.0$). 40
3.11 Variation of pitch angle (γ) with shear rate (η) for different values of the gas mass fraction ϵ. The top row corresponds to the stellar component, while the bottom row represents the gaseous component. Each subplot shows results for a fixed β_s and β_g. Different colored curves denote different values of gas mass fraction ϵ, while the gas scale height is kept fixed ($\beta_g = 0.1$). In all cases, the pitch angle decreases with increasing shear rate, indicating more tightly wound spiral structures at higher differential rotation. 41
3.12 The exponential decay of pitch angle with shear rate for the two-fluid case, shown for different values of gas mass fraction (ϵ) and disc scale height, with ($Q_s = 1.8, Q_g = 1.2$) 42

Chapter 1

Introduction

1.1 Occurrence of Spiral arm in real galaxies

Spiral arms are among the most common non-axisymmetric structures observed in disc galaxies, second only to stellar bars. Approximately 60 percent of galaxies in local Universe are spiral galaxies (Buta, 1989). Observations in the local Universe show that spiral arms are present in a wide variety of disc galaxies and exhibit a broad range of morphologies as shown in Figure 1.1, from well-organized grand-design patterns to fragmented and flocculent structures (e.g. Debra Meloy Elmegreen and Bruce G Elmegreen, 2013; Yu et al., 2018; Savchenko et al., 2020). Similar spiral features have also been identified in galaxies observed out to redshifts of $z \sim 1.4 - 1.8$, indicating that spiral structure is already well established at earlier cosmic times (e.g. Debra Meloy Elmegreen and Bruce G Elmegreen, 2013; Willett et al., 2017; Hodge et al., 2019).

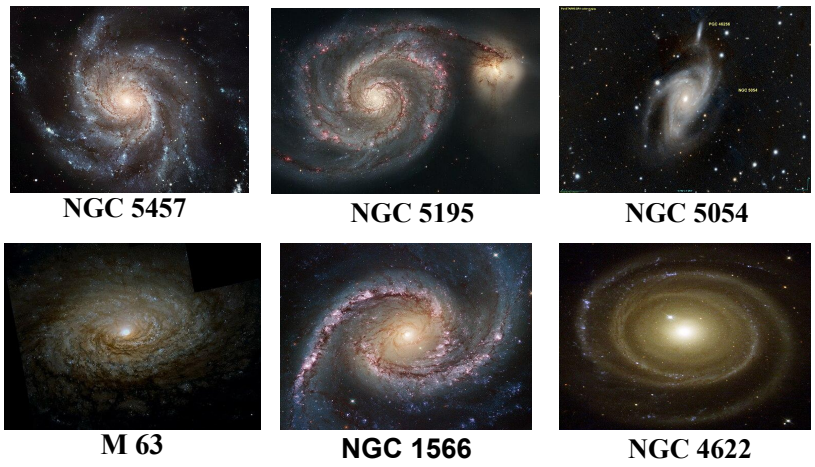


Figure 1.1: Examples of disc galaxies showing a wide range of spiral morphologies. This sample includes grand-design spirals such as NGC 5194 (M51) and NGC 1566, multi-armed and intermediate spirals like NGC 5054 and M 63, as well as galaxies with unusual or counter-winding spiral structures such as NGC 4622. *Image credits:* HST, PanSTARRS.

Spiral galaxies exhibit a wide range of spiral morphologies such as grand-design spiral galaxies that are characterized by two prominent and symmetric spiral arms that extend over a large fraction of the galactic disc. These arms are frequently connected to stellar bars or induced by tidal interactions with companion galaxies. Such systems typically possess massive and dynamically cold disc in which the ordered rotational motion dominates over random stellar motions. Under these conditions, large-scale non-axisymmetric perturbations can persist for long times, leading to strong, coherent, and long-lived spiral patterns.

Multi-armed spiral galaxies represent an intermediate morphological class. They contain several spiral arms that are coherent over limited radial ranges but do not exhibit a single global two-armed symmetry. These structures are often interpreted as transient

and recurrent features produced by internal disc processes such as swing amplification, where small perturbations are amplified by the combined effects of differential rotation and disc self-gravity. As a result, multi-armed spirals are common in disc that are marginally stable and capable of sustaining repeated spiral activity (e.g. Toomre, 1964; Goldreich and Lynden-Bell, 1965; Toomre, 1981).

Flocculent spiral galaxies display the most irregular spiral structure, consisting of short and patchy arm segments without a well-defined global pattern. These features are primarily associated with local gravitational instabilities, particularly in the gas rich disc, rather than global stellar density waves (DEBRA MELOY Elmegreen and BRUCE G Elmegreen, 1984). Flocculent spirals are commonly found in isolated galaxies with dynamically warm stellar disc, where large random stellar motions suppress the formation of coherent large-scale spiral modes. Observational classifications show that these galaxies lack coherent large-scale spiral modes and instead exhibit fragmented arm features distributed across the disc(B. G. Elmegreen, 1995; C. Dobbs and Baba, 2014).

Observational studies by D. M. Elmegreen and B. G. Elmegreen (1987) demonstrated that grand-design spirals are more common in massive and dynamically cold disc, often influenced by bars or tidal interactions, whereas flocculent structures are preferentially found in isolated galaxies dominated by local gravitational instabilities. This diversity of spiral morphologies highlights the strong dependence of spiral structure on disc stability, kinematic temperature, gas content, and external perturbations. Several physical mechanisms have been proposed to explain the origin and evolution of spiral arms. In the classical density wave theory, spiral arms are described as long-lived, quasi-stationary wave patterns that rotate with a fixed pattern speed and compress gas as disc material passes through the arms, thereby enhancing star formation (Lin and Frank H. Shu, 1964a). In contrast, the swing amplification mechanism explains spiral arms as transient features produced by the amplification of leading perturbations into trailing spirals due to the combined effects of differential rotation, pressure, self-gravity, and disc shear (Toomre, 1981). This mechanism naturally produces recurrent and multi-armed spiral patterns, as commonly seen in numerical simulations and observations (Toomre, 1964; Toomre, 1981; Chanda J. Jog, 1992). Overall, observational and theoretical studies across cosmic time indicate that spiral arms do not arise from a single universal mechanism. Instead, their morphology, strength, and lifetime depend sensitively on disc properties such as mass distribution, gas fraction, velocity dispersion, and the presence of bars or external perturbations. Understanding the formation and evolution of spiral arms therefore provides crucial insight into the dynamical state and evolutionary history of disc galaxies.

1.2 Multi-Wavelength appearance of Spiral arms in galaxies

Spiral arms are complex structures, composed of stars, gas and dust, and their appearance depends strongly on the wavelength at which they are observed. Different stellar populations emit at different wavelengths across the electromagnetic spectrum from gamma rays to radio rays. Therefore, multi-wavelength observations are essential for constructing a complete picture of galaxy. Certain properties of spiral structure vary with the chosen wavelength, since observations at different wavelengths trace different constituents of the galactic disc, including stellar populations, atomic and molecular gas, dust, and high-energy processes. As a result, the appearance, strength, and continuity

of spiral arms can differ across the electromagnetic spectrum. In the X-ray regime, observations of spiral galaxies reveal the presence of very high, energetic components that are invisible at optical wavelengths. X-ray images typically show a combination of diffuse emission and bright compact sources. The diffuse X-ray emission is the regions filled with hot interstellar gas at very high temperatures of 10^6–10^8 K, produced by supernova explosions and stellar winds from massive stars. In many spiral galaxies, this diffuse component extends above and below the disc, forming an halo (Strickland et al., 2004). The X-Ray emission is particularly strong, revealing powerful galactic outflows and winds driven by supernova activity. Thus, X-ray observations provide a view of spiral galaxies dominated by energetic processes (Fabbiano, 1989). Ultraviolet (UV) emission traces even younger stellar populations and therefore provides a direct view of ongoing star formation. UV observations tend to show the spiral arms as more fragmented and irregular than in optical light (Calzetti et al., 2007). UV emission is effective tracers of star formation triggered by density enhancements and spiral shocks (Tamburro et al., 2008; Foyle, Rix, C. L. Dobbs, A. K. Leroy, et al., 2011). Optical wavelengths trace young, massive stars. As these stars are bright and short-lived, optical images highlight regions of recent star formation along the spiral arms (R. C. Kennicutt, 1998). These young stellar populations often outline the arms in a clumpy way, reflecting star formation occurring in localized regions. However, dust extinction and the dominance of massive stars mean that optical images do not accurately represent the total stellar mass distribution. In contrast, near-infrared (NIR) wavelengths trace older, cooler stellar populations that dominate the stellar mass in the disc. Since NIR light is less affected by dust extinction, NIR images reveal the smooth and continuous underlying structure of spiral arms (Kormendy and Robert C. Kennicutt, 2004). Thus, NIR observations are crucial for distinguishing between spiral features caused by gravitational perturbations and those arising purely from star formation. Mass-mapping studies using NIR also show that some galaxies host long-lived, global spiral modes (Meidt et al., 2013).
These multi-wavelength comparisons also reveal differences between spiral galaxy types. Grand-design spirals tend to show strong spatial order between CO, dust, and star-forming regions, while flocculent spirals show more stochastic star formation and less coherent gas flows (D. M. Elmegreen and B. G. Elmegreen, 1987; B. G. Elmegreen, 1995). In multi-armed disc, the molecular gas and star formation activity are more locally driven by turbulence and gravitational instability rather than global density waves. Taken together, all these observations show that spiral arms are not simply high intensity star-forming structure. Instead, they are dynamical structures that organize the flow of interstellar gas and stellar mass, influence where new stars form. Multi-wavelength analysis provides crucial insight into how spiral structure shapes both the stellar distribution and the star formation history of galactic disc.

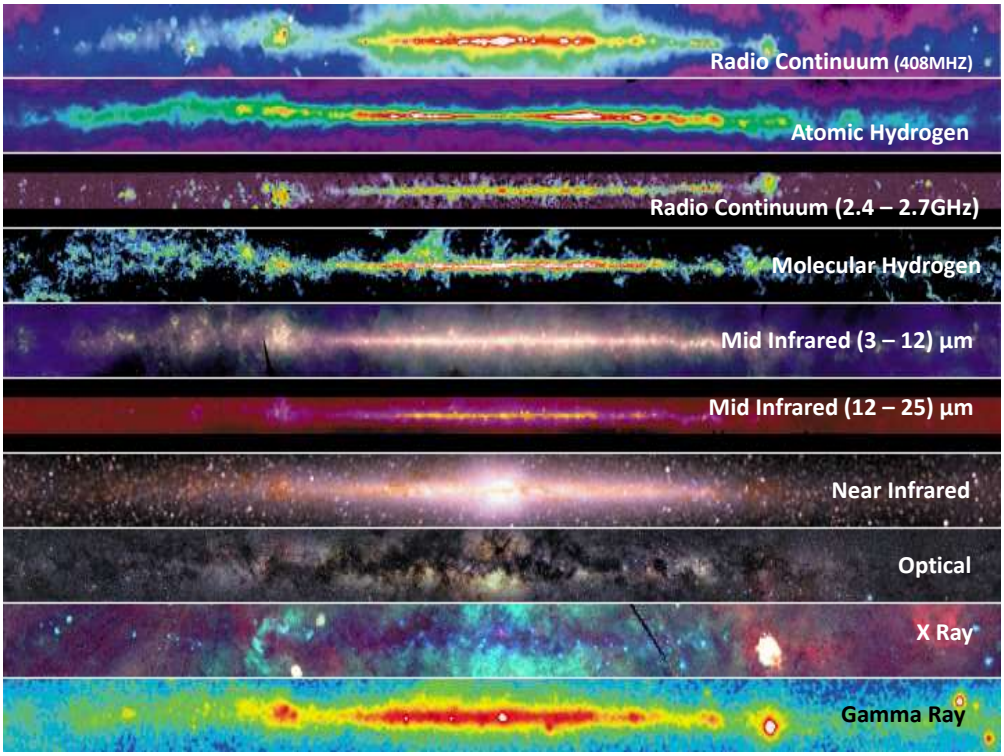


Figure 1.2: *One galaxy many faces:* the Milky Way viewed at ten different wavelength regimes from radio to gamma rays, illustrating how different spectral bands trace distinct physical component of galactic disc. In this map the central part of the galaxy in a band that extends up to 10° north and 10° south of the galactic plane (NASA Goddard Space Flight Center, 2010).

Our own Milky Way shows very different structures when observed at different wavelengths of the electromagnetic spectrum as shown in Figure 1.2, with each band tracing distinct physical components of the galactic disc. Low-frequency radio continuum emission at 408 MHz is dominated by radiation from high-energy electrons moving through the interstellar magnetic field, with strong emission produced near supernova remnants where shock waves accelerate particles to relativistic speeds. Observations of atomic hydrogen using the 21-cm line trace the column density of neutral gas in the cold and warm interstellar medium, revealing large-scale diffuse gas clouds distributed across the disc. Higher-frequency radio continuum observations at 2.4–2.7 GHz provide improved angular resolution and highlight emission from hot ionized gas and energetic electrons, allowing individual Galactic objects to be seen more clearly. Molecular hydrogen is traced indirectly through the transition of carbon monoxide, which maps dense molecular clouds concentrated along spiral arms and associated with active star formation. Infrared observations probe thermal emission from interstellar dust, with far and mid-infrared bands tracing dust heated by starlight in star-forming regions, while near-infrared emission primarily traces older stellar populations with reduced effects of dust extinction. Optical observations are dominated by visible light from stars but are strongly affected by absorption and scattering by interstellar dust, limiting the view mostly to regions near the Sun. Ultraviolet emission is not shown as a full-sky map due to its relatively featureless appearance, while X-ray observations reveal hot, shocked gas and supernova remnants, with absorption by cooler gas producing shadowed regions. At the highest energies, gamma-ray emission traces interactions between cosmic rays and interstellar gas, as well as compact high-energy sources such as pulsars. Together, these maps demonstrate that a multi-wavelength approach is essential for obtaining a

complete physical picture of the structure and energetic processes within the Milky Way galaxy.

1.3 Properties of Spiral arm

Spiral arms have several key properties that we can observe and measure to understand their structure. The three most fundamental parameter of these are the spiral arm multiplicity, strength, and the pitch angle. Each parameter reveals different aspects of spiral arm formation, evolution, and interaction with the surrounding galactic components.

1.3.1 Spiral arm multiplicity

Spiral arm multiplicity refers to the number of distinct spiral arms in any disc galaxy. Observationally, a galaxy is said to possess m-fold rotational symmetry if its face-on surface brightness distribution $I(R, \phi)$ satisfies $I(R, \phi + 2\pi/m) = I(R, \phi)$; in this case the galaxy is described as having m arms (Binney and Tremaine, 2008). This condition can be quantified through a Fourier decomposition of the azimuthal surface brightness profile,

$$\frac{I(R,\phi)}{\bar{I}(R)} = 1 + \sum_{m=1}^{\infty} A_m(R) \cos m[\phi - \phi_m(R)] \,, \tag{1.1}$$

where

$$\bar{I}(R) = \frac{1}{2\pi} \int_0^{2\pi} I(R,\phi)\, \mathrm{d}\phi \tag{1.2}$$

is the azimuthally averaged surface brightness at galactocentric radius R, and $A_m(R)$ and $\phi_m(R)$ are the amplitude and phase of the m-th Fourier component, respectively (Binney and Tremaine, 2008). The dominant spiral arm multiplicity is then identified as the value of m that maximises the radially averaged Fourier amplitude over a specified range of galactocentric radius.

Observational surveys using near-infrared (NIR) imaging — which traces the underlying stellar mass distribution rather than regions of recent star formation — have established that most grand-design spirals possess approximate two-fold rotational symmetry, with the $m = 2$ mode dominating the surface density. Grand-design spirals with $m \neq 2$ are rare. A significant fraction of disc galaxies exhibit lopsided distortions with $A_1 \gtrsim 0.2$ in their outer regions, and careful Fourier decompositions occasionally reveal three-armed patterns; however, the near-universal dominance of two-armed patterns in grand-design spirals is a striking observational fact that demands explanation from any successful theory of spiral structure (Binney and Tremaine, 2008).

1.3.2 Strength of Spiral arms

The strength of spiral structure in a disc galaxy quantifies how prominent the non-axisymmetric spiral pattern is relative to the underlying smooth disc. For an m-armed spiral, the amplitude $A_m(R)$ from the Fourier decomposition of Eq. 1.1 provides a direct, radially resolved measure of this contrast. If a single Fourier mode dominates the spiral, its strength can also be expressed through the arm-to-interarm surface brightness ratio K, which is related to the Fourier amplitude by



(a) Milky Way (b) M101 (c) NGC 2775

Figure 1.3: Examples of different spiral-arm multiplicity. (a) shows a grand-design spiral galaxy, Milky Way galaxy (b) illustrates a multi-arm spiral galaxy, and panel (c) represents a flocculent spiral galaxy, revealing the wide range of structures observed in spiral systems across the local universe. *Image credits:* HST, NASA/JPL-Caltech.

$$K = \frac{1 + A_m}{1 - A_m}, \tag{1.3}$$

(Binney and Tremaine, 2008). A value of $K = 1$ corresponds to a perfectly axisymmetric disc with no spiral contrast, while larger values of K indicate progressively stronger spiral patterns.

Observations of grand-design spirals in near-infrared light, which traces the stellar mass distribution rather than transient star-forming regions, yield amplitude values in the range $0.15 \lesssim A_2 \lesssim 0.6$, corresponding to arm-to-interarm surface brightness ratios of $1.4 \lesssim K \lesssim 4$. These measurements confirm that spiral arms represent genuine density enhancements in the old stellar disc, and are not merely regions of recent star formation.

1.3.3 Pitch angle

The pitch angle is the fundamental morphological parameter that quantifies how tightly or loosely a spiral arm wound. It is defined as the angle between the tangent to the spiral arm at a given point and the circle of constant galactocentric radius R passing through that point; by convention $0 < \gamma < 90°$ for trailing arms (Binney and Tremaine, 2008). In Figure 1.4 the red curve represents the spiral arm, while the blue circle corresponds to a circle of constant galactocentric radius R.

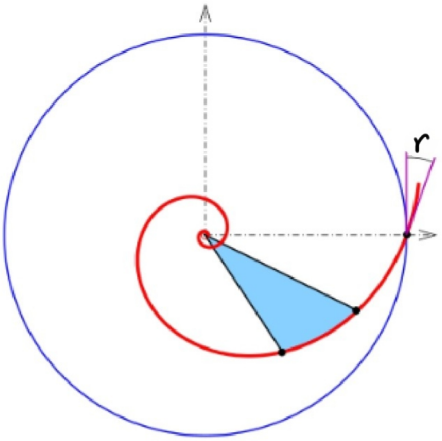


Figure 1.4: Pitch angle γ of a spiral arm. The pitch angle is defined as the angle between the tangent to the spiral (red curve) and concentric circle around galactic center (blue circle).

Mathematical definition

The locus of an m-armed spiral pattern can be written in the compact form

$$m\phi + f(R,\, t) = \text{constant} \pmod{2\pi}, \tag{1.4}$$

where $f(R, t)$ is the shape function of the spiral. The radial wavenumber is defined as

$$k(R,\, t) \equiv \frac{\partial f(R,\, t)}{\partial R}, \tag{1.5}$$

and its sign distinguishes leading from trailing arms:

$$k < 0 \;\Leftrightarrow\; \text{leading arm}, \qquad k > 0 \;\Leftrightarrow\; \text{trailing arm}. \tag{1.6}$$

The pitch angle is then related to the wavenumber by

$$\cot\gamma = \frac{kR}{m}, \tag{1.7}$$

(Binney and Tremaine, 2008). Since $|kR| \gg 1$ for tightly wound arms, Eq. 1.7 implies $\alpha \ll 1$, consistent with observations.

Variation along the Hubble sequence

Observationally, the pitch angle varies systematically with galaxy morphology along the Hubble sequence. Early-type spirals (Sa, Sb) possess tightly wound arms with small pitch angles, while late-type spirals (Sc, Sd) exhibit more open patterns with larger pitch angles (Binney and Tremaine, 2008). A sample of nearby spiral galaxies shows that the typical pitch angle lies in the range $\gamma \simeq 10°$–$15°$, with considerable scatter at each Hubble type (Binney and Tremaine, 2008). This systematic trend arises because early-type spirals generally have more massive bulges and stronger central mass concentrations, which drive stronger differential rotation and therefore larger shear rates in the disc. Thus, the pitch angle generally increases from early-type to late-type spiral galaxies along the Hubble sequence. This trend is clearly illustrated in Figure 1.5, which shows the Hubble tuning fork diagram moving from early-type spirals (Sa) to late-type spirals (Sc) along the sequence, the spiral arms visibly transition from tightly wound to more open structures. This morphological change directly reflects the increase in pitch angle. In particular, the Sa galaxies exhibit small pitch angles consistent with tightly wound arms, whereas Sc galaxies show larger pitch angles corresponding to loosely wound spiral patterns. Thus, the figure provides a visual confirmation of the systematic variation of pitch angle along the Hubble sequence.

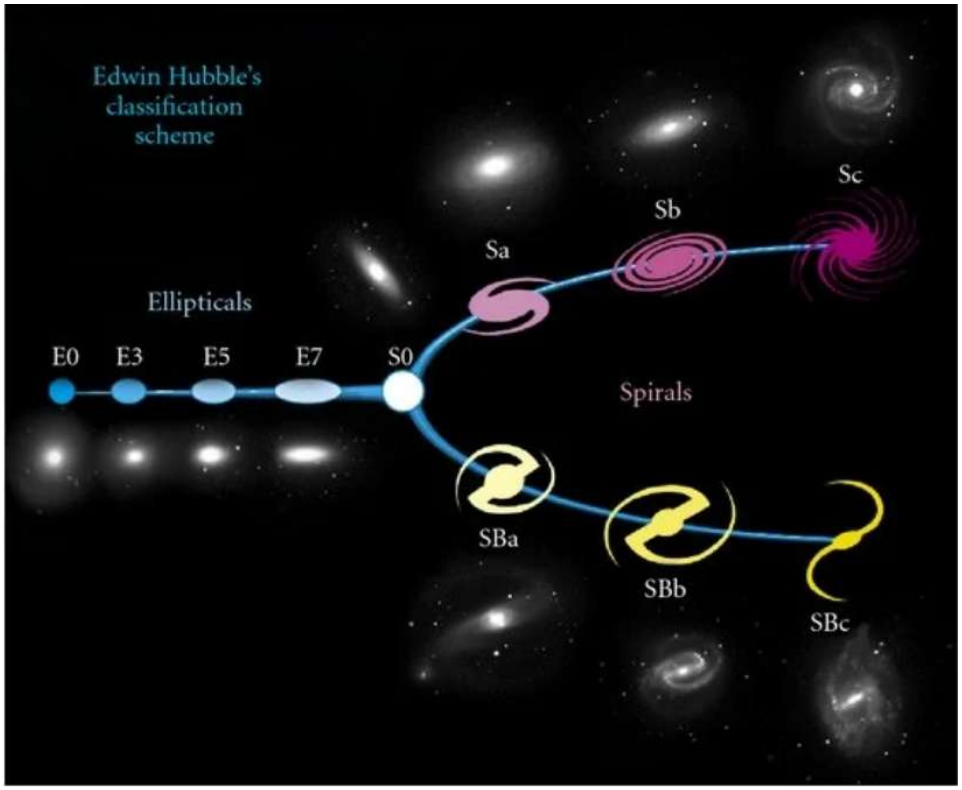


Figure 1.5: Schematic representation of the Hubble tuning fork diagram showing the morphological classification of galaxies. The sequence begins with elliptical galaxies ranging from E0 to E7, followed by lenticular galaxies (S0) at the junction point. From S0, the sequence bifurcates into normal spiral galaxies (Sa, Sb, Sc) and barred spiral galaxies (SBa, SBb, SBc). Along both spiral branches, the bulge size decreases and the spiral arms become more open and loosely wound from early-type to late-type galaxies *Image credits:* NASA and ESA

1.3.4 The pitch angle vs shear relation and its discrepancies

Observational result: The Empirical Correlation

The systematic evidence linking pitch angle to shear rate came from large observational surveys. Analyzing a sample of nearby grand-design spiral galaxies, (M. S. Seigar et al., 2005; Marc S. Seigar et al., 2006) measured pitch angles using two-dimensional Fourier techniques and derived shear parameters directly from observed rotation curves. They found a clear linear, inverse trend:

$$\gamma = (64.25 \pm 2.87) - (73.24 \pm 5.53)\,\eta \tag{1.19}$$

where their observationally-defined shear parameter is $\eta = \frac{1}{2}\left(1 - \frac{R}{V}\frac{dV}{dR}\right)$. This result solidified the intuitive idea: galaxies with stronger differential rotation (higher shear) exhibit more tightly wound spiral arms. However, as a purely empirical fit, this relation did not emerge from a dynamical model of arm formation and assumed a simplified, single-component disc.

The quantity η_S is a dimensionless shear parameter that quantifies how rapidly the angular velocity $\omega(R)$ of a galactic disc changes with radius. This expression is introduced by (Goldreich and Lynden-Bell, 1965) while studying the local stability of differentially rotating galactic disc.

Theoretical & Numerical result

In parallel, theoretical efforts derive the relationship between spiral arm pitch angle and shear rate from within the framework of swing amplification. Using high-resolution local N-body simulations of a collisionless, infinitesimally thin stellar disc, (Michikoshi and Kokubo, 2014) investigated the nonlinear evolution of perturbations in a shearing sheet. Their analysis produced a distinct, non-linear prediction:

$$\tan\gamma = \frac{2}{7}\sqrt{\frac{4-2\eta}{\eta}} \tag{1.18}$$

where $\eta = -d\ln\Omega/d\ln R$ is the local shear rate. This was a significant result, demonstrating that the pitch angle is an intrinsic outcome of the swing amplification process, where the timescale for a leading wave to swing to trailing—and reach peak amplification—is set by the epicyclic motion and shear (Grand, Kawata, and Cropper, 2013; Ghosh and Chanda J Jog, 2018)

1.4 Density wave theory

Density wave theory, first developed by C. C. Lin and Frank Shu in the 1960s, resolved a long-standing problem in galactic astronomy, the "winding dilemma." Since galaxies rotate differentially-the inner regions rotate faster than the outer ones—any material spiral pattern would wind up and disappear within a few rotations. Lin and Shu proposed that spiral arms are not made of fixed stars but instead represent quasi-stationary spiral structures(QSSS), or long-lived, rotating patterns of enhanced density that persist over many galactic rotations. These waves act like traffic jams on a highway, individual stars move in and out of the arms, but the spiral pattern itself remains stable (Lin and Frank H. Shu, 1964b; Frank H Shu, 2016). Below Figure 1.6 illustrates this wave-like structure.

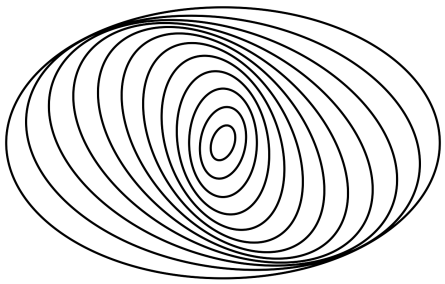


Figure 1.6: Spiral arms as density waves. The pattern remains stable over time despite differential rotation, analogous to a traffic jam where individual cars move through but the congestion persists (Image: Wikipedia).

According to density wave theory, the spiral arms are gravitational density waves that rotate around the galaxy with a fixed pattern speed, denoted by Ω_p. This pattern speed is different from the local circular speed Ω_R of the stars and gas within a given radius R of the galactic disc. Stars and gas clouds move in and out of the spiral pattern as they orbit the galactic center. When they pass through the denser region of the wave, their motion slows down because of the gravitational attraction of the spiral arm and, they feel some extra pressure because the star formation rate in this high density region increases. This leads to a temporary buildup of matter, creating a visible spiral arm. As stars and gas leave the spiral arm, they speed up again and move ahead, while new material enters from behind. In this way, the spiral pattern can maintain its shape even though individual stars and gas clouds are constantly moving.
Thus, the spiral arm is maintained as a self-sustained wave pattern, while individual stars and gas clouds do not remain permanently in the arms but continuously stream through them. This allows the spiral pattern to remain relatively stable and long-lived, even though the underlying mass distribution is in motion.

1.4.1 Limitations of the density wave theory

Despite its success in explaining the presence of spiral arms in a few galaxies, the density wave theory has several limitations.

1. Origin and persistence of spiral
   The theory assumes that spiral arms are long-lived, quasi-stationary wave patterns. However, it does not provide a precise physical mechanism for how such waves are initially generated or how they are sustained over several galactic rotation periods (e.g. Lin and Frank H. Shu, 1964b; Bertin and Lin, 1996; Sellwood and Carlberg, 1984; Sellwood, 2011; C. L. Dobbs and Baba, 2014)

2. **Limited morphologies**
   Density wave theory naturally predicts two-armed (grand-design) spiral patterns. However, many spiral galaxies exhibit multi-armed structures that lack symmetry (e.g. Toomre, 1981; D. M. Elmegreen and B. G. Elmegreen, 1982; C. L. Dobbs and Pringle, 2010).

3. **Star formation offset spiral arm**
   This theory suggests that gas is compressed as it enters a spiral arm, creating dust lanes first, followed by molecular clouds, and subsequently regions of active star formation. Consequently, a clear spatial separation between these features is expected along the spiral arm.(Foyle, Rix, C. L. Dobbs, A. Leroy, et al., 2011; Kreckel, Blanc, Schinnerer, et al., 2016).

4. **Inconsistency with observed pattern speeds**
   The density wave theory predicts that spiral patterns rotate with a constant pattern speed (Ω_p), distinct from the disc rotation speed. However, this prediction has been challenged by several observational studies (e.g. Merrifield and Kurosawa, 2000; Chandar et al., 2016; Schinnerer et al., 2017; Shabani et al., 2018).

Therefore, density wave theory alone is insufficient to explain the full dynamical behaviour of spiral arms, and additional mechanisms such as swing amplification (Toomre, 1981), bar-driven spirals Sellwood and Sparke (1988), and tidal interactions Oh et al.

(2015), required to provide a more complete description of spiral arm formation and evolution.

1.5 Swing Amplification

The swing amplification mechanism explains how spiral arms can form and grow in disc galaxies without requiring the arms to be permanent or long-lived. Unlike the classical density wave theory, which assumes that spiral arms are long-lived wave patterns with a constant pattern speed, the swing amplification mechanism predicts spiral features that are short-lived and continuously regenerated by differential rotation over time. (e.g. Goldreich and Lynden-Bell, 1965; Julian and Toomre, 1966; Toomre, 1981; Athanassoula, 1984; Chanda J. Jog, 1992; Fuchs, 2001; D'Onghia, Vogelsberger, and Hernquist, 2013; Ghosh and Chanda J Jog, 2014; Michikoshi and Kokubo, 2016; Ghosh and Chanda J Jog, 2018). This idea is strongly supported by modern N-body simulations (Sellwood, 2011; Baba, Saitoh, and Wada, 2013; C. Dobbs and Baba, 2014; Michikoshi and Kokubo, 2014). These studies have revealed many useful insights about the spiral structure and its role in the secular evolution of the galactic disc. The efficiency and evolution of swing amplification in galactic disc are determined by the combined effects of shear rate, epicyclic motion, self-gravity and pressure.

1.5.1 Effect of shear rate in swing amplification

Galactic disc rotate differentially. This differential rotation a *shear* in the galactic disc. Shear stretches any perturbation into a spiral form. As a result, an initially small density perturbation first appears as a leading spiral pattern and subsequently evolves into a trailing spiral structure. Swing amplification takes advantage of this stretching process. The disturbance naturally changes from a leading shape to a trailing shape, and the trailing shape is the one that experiences swing amplification (Toomre, 1981; Sellwood, 2014). Thus, shear is essential for changing a small perturbation into spiral arms.

1.5.2 Effect of epicyclic motion in swing amplification

Stars in a galactic disc do not follow a perfectly circular motion. Instead of circular motion, they execute small oscillations around their mean circular paths. These oscillations are known as *epicyclic motion*. The frequency associated with this motion is referred to as the *epicyclic frequency* (κ), given by:

$$\kappa^2 = R\frac{\mathrm{d}\Omega^2}{\mathrm{d}R} + 4\Omega^2 \tag{1.8}$$

where $\Omega(R)$ is the angular frequency of the disc at radius R. The quantity κ characterizes how rapidly stars oscillate radially about their guiding center orbits.

During swing amplification, when a small perturbation in density arises, the epicyclic motion of stars plays an important role in determining how the disc responds. Instead of stars oscillating independently, their motions can become *correlated* in the presence of a perturbation. This correlation leads to a temporary increase in the local surface density and thereby enhances the spiral feature. Physically, the epicyclic motion provides a restoring force that prevents the disturbance from collapsing immediately under self-gravity. Simultaneously, it allows the perturbation to last long enough for differential

rotation (shear) to convert it from a leading to a trailing position, during which the amplification is strongest. The density response of the disc is enhanced when the perturbation frequency ω satisfies:

$$\omega \approx m\Omega \pm \kappa, \tag{1.9}$$

where m is the azimuthal wave number. This condition represents a situation where the stellar orbits move *in phase* with the perturbation (Julian and Toomre, 1966; Toomre, 1981). Thus, epicyclic motion contributes to swing amplification in two significant ways: The efficiency of this process depends sensitively on the ratio κ/Ω. For disc with nearly flat rotation curves, where $\kappa/\Omega \approx 1.4$, swing amplification becomes particularly effective (Binney and Tremaine, 2008).

1.5.3 Effect of self gravity on swing amplification

Spiral structures in disc galaxies are due to gravitational instabilities that arise due to differential rotation of the galactic disc. Self-gravity plays a crucial role in determining whether small density perturbations can grow into amplified spiral structures as they are sheared by the differential rotation of the galactic disc. The strength of self-gravity in the disc is quantified by the *Toomre stability parameter* (Q), which provides a direct measure of the disc gravitational instability. A perturbation that initially has a *leading* orientation is gradually wound up and transformed into a *trailing* configuration as time evolves and such perturbation would be dispersed due to pressure and therefore not result in any permanent spiral arm. When a perturbation creates a change in the local surface density, the gravitational force associated with this density begins to draw surrounding material toward it. During the phase when the perturbation swings from leading to trailing, self gravity dominate over pressure. As a result, the perturbation may undergo a growth. This growth is quantified by the *maximum amplification factor* (MAF). The magnitude of the MAF depends directly on the strength of the disc self-gravity: stronger self-gravity produces stronger amplification and more prominent spiral patterns. The strength of self-gravity is opposing stability factor such through the Toomre stability factor. For a stellar disc, it is defined as (Toomre, 1964)

$$Q = \frac{\kappa\sigma}{3.36G\Sigma}, \tag{1.10}$$

and for a gaseous disc Q is defined as

$$Q = \frac{\kappa c_g}{\pi G\Sigma}, \tag{1.11}$$

where, σ (or c_s) is the velocity dispersion and sound speed respectively, G is the gravitational constant and Σ is the surface mass density of the disc.

The Toomre parameter expresses the balance between the stabilizing (pressure and epicyclic motion) and destabilizing force (self-gravity). A smaller value of Q indicates stronger self-gravity relative to pressure and epicyclic motion. Hence optimal condition for swing amplification, while a larger value of Q indicates that stabilizing the perturbation itself. The efficiency of swing amplification varies systematically with Q, when $Q \approx 1$, the disc is marginally stable. Self-gravity is strong enough to amplify perturbations significantly, In this region, swing amplification is most efficient, producing very strong spiral arms. however $Q > 1.6 - 2$, the disc becomes stable. Pressure suppresses gravitational amplification, and perturbations are sheared apart before they can grow. The resulting disc appears smoother and lacks of spiral arm.

1.5.4 *Effect of pressure on swing amplification*

Pressure in a galactic disc originates from the random motions of stars and gas. Pressure prevents material from collapsing. If the pressure is too high, perturbation cannot grow, the material collapses instead of forming spiral arms. Swing amplification occurs when pressure is dominated by self-gravity (Goldreich and Lynden-Bell, 1965; C. L. Dobbs, Theis, et al., 2013). After some time, the spiral arm fades as pressure again overtakes the self gravity. However, new disturbances continuously form, so the disc always shows spiral features. This explains why spiral arms can appear even though individual arms are constantly forming and dissolving (Sellwood, 2011; Baba, Saitoh, and Wada, 2013). Therefore, swing amplification is widely considered a fundamental mechanism behind spiral structure in many disc galaxies (C. L. Dobbs and Baba, 2014).

1.6 *Scientific Goal of my Work*

Previous observational and theoretical studies have established some correlation between the spiral arm pitch angle and the shear rate in galactic discs. Observational studies have identified a linear trend in which the pitch angle decreases with increasing shear rate, implying that spiral arms become more tightly wound in regions of strong differential rotation (M. S. Seigar et al., 2005; Marc S. Seigar et al., 2006). Similarly, theoretical studies have reported an inverse dependence between pitch angle and shear rate, concluding that stronger shear produces more tightly wound spiral structures (Michikoshi and Kokubo, 2014). Despite these results, there is still no consistent theoretical understanding of how the spiral arm pitch angle depends on disc shear. In particular, the discrepancy between observationally pitch angles and theoretical predictions remains unresolved. Most previous studies have considered only infinitesimally thin stellar discs and have neglected the important dynamical roles played by finite disc thickness and interstellar gas. Since the shear rate is determined by the underlying mass distribution and rotation curve of the galaxy, any relation between pitch angle and shear provides an important connection between the observed morphology of spiral galaxies and the internal dynamics of galactic discs. Understanding this relation is therefore essential for explaining why different galaxies exhibit different spiral morphologies, ranging from tightly wound grand-design spirals to loosely wound multi-armed and flocculent systems. The pitch angle of the amplified spiral arm depends on the time at which the perturbation reaches its maximum growth (radial mode to trailing mode). However, most of studies have assumed an infinitesimally thin stellar disc, which is not an enough representation of real galaxies. Both the stellar and gaseous components possess finite vertical scale heights, which reduce the effective self-gravity of the disc and therefore influence the growth of non-axisymmetric perturbations. A thicker disc weakens the gravitational coupling between different regions of the disc and suppresses the efficiency of swing amplification. However, the detailed dependence of the pitch angle on the disc thickness has not yet been systematically explored over a wide range of galactic parameters. In addition to finite thickness, the presence of interstellar gas is expected to play a crucial role in determining the morphology of spiral arms. Even a modest gas fraction can significantly modify the overall stability of the disc, enhance the growth of perturbations, and alter the resulting spiral structure. In real galaxies, stars and gas are gravitationally coupled and evolve together. Therefore, a realistic study of spiral arm morphology requires a two-fluid description in which both the stellar and

gaseous components are included self-consistently.

To address these issues, this work investigates the dependence of spiral arm pitch angle and strength (MAF) in galactic discs within the framework of swing amplification theory. We first consider a one-fluid galactic disc consisting only of a fluid component. This allows us to isolate the role of stellar self-gravity and examine how the pitch angle varies with shear rate, Toomre stability parameter, wavelength parameter, and finite disc thickness parameter. In this one-fluid model, we study both infinitesimally thin and finite-thickness stellar discs in order to quantify how vertical structure influences the amplification of spiral perturbations. Further, we extend the analysis to a more realistic two-fluid galactic disc consisting of stars and interstellar gas. In this model, the stellar and gaseous components are treated as gravitationally coupled fluids, each characterized by its own Toomre parameter, velocity dispersion, and scale height. This approach allows us to investigate how the combined effects of shear, finite thickness, and interstellar gas determine the resulting spiral arm morphology. The main objective of this work is therefore to develop a more physically realistic description of the relation between spiral arm pitch angle and galactic disc shear. By including finite thickness and gas in the framework of swing amplification, we aim to understand whether these additional effects can help reconcile the discrepancy between previous theoretical predictions and observations. In summary, this work seeks to understand how the interplay between differential rotation, self-gravity, finite disc thickness, and interstellar gas shapes the morphology of spiral arms in galaxies.

Chapter 2

Formulation of swing amplification in disc galaxies

2.1 One-fluid galactic disc with finite thickness

The formulation that is used here is swing amplification. The formulation for the swing amplification is explained below:

Local perturbations characterised by a wavelength smaller than the galactocentric radial distance are analysed. The perturbations are assumed to be planar, and the length of the perturbation is greater than the scale height of the disc. In the mathematical framework, i=s and i=g describe the equation for star and gas, respectively.

The general form of the Euler equation governing fluid motion can be written as

$$\frac{\partial \mathbf{V}}{\partial t} + (\mathbf{V}\cdot\nabla)\mathbf{V} = -\frac{1}{\rho}\nabla P - \nabla\Phi \tag{2.1}$$

$$\underbrace{\frac{\partial \mathbf{V}}{\partial t}}_{\text{Local acceleration}} + \underbrace{(\mathbf{V}\cdot\nabla)\mathbf{V}}_{\text{Convective acceleration}} = - \underbrace{\frac{1}{\rho}\nabla P}_{\text{Pressure gradient force}} - \underbrace{\nabla\Phi}_{\text{Gravitational force}}$$

The galactic disc undergoes differential rotation; therefore, the fluid equations are most conveniently expressed in a rotating reference frame, where the Euler equation modified by the presence of coriolis and centrifugal forces

$$\frac{\partial \mathbf{V}}{\partial t} + (\mathbf{V}\cdot\nabla)\mathbf{V} = -\frac{c^2}{\Sigma}\nabla\Sigma - \nabla\Phi - 2\boldsymbol{\Omega}\times\mathbf{v} + \boldsymbol{\Omega}^2\mathbf{R} \tag{2.2}$$

In the formulation of the rotating galactic disc, the quantity $\mathbf{V}$ represents the two-dimensional velocity with respect to the rotating axes. The rotation of the frame itself characterized by the angular velocity vector $\boldsymbol{\Omega}$. The term $\boldsymbol{\Omega}^2\mathbf{r}$ represents the centrifugal force, while $2\boldsymbol{\Omega}\times\mathbf{V}$ corresponds to the coriolis force.

A cartesian coordinate system (x, y, z) is defined with its center at (R_0, ϕ_0), and unit vectors $\hat{i}, \hat{j}, \hat{k}$ such that $\hat{i}$ coincides with the initial outward radial direction. The non-axisymmetric perturbation analysis is then carried out within this local region.
The local, linear perturbed Euler equation in Cartesian coordinates is given by

$$\frac{\partial v_x}{\partial t} + 2Ax\frac{\partial v_x}{\partial y} - 2\Omega v_y = -\frac{\partial\Phi}{\partial x} - \frac{c^2}{\Sigma_0}\frac{\partial}{\partial x}(\delta\Sigma) \tag{2.3}$$

$$\frac{\partial v_y}{\partial t} + 2Ax\frac{\partial v_y}{\partial y} + 2Bv_x = -\frac{\partial\Phi}{\partial y} - \frac{c^2}{\Sigma_0}\frac{\partial}{\partial y}(\delta\Sigma) \tag{2.4}$$

where A and B are the Oort's constants, v_x and v_y denote the perturbed velocities, Σ_0 and $\delta\Sigma$ represent the unperturbed and perturbed surface densities and Φ is the gravitational potential of the fluid disc.

The linear perturbation equations corresponding to the continuity and Poisson equations are given by

$$\frac{\partial}{\partial t}(\delta\Sigma) + 2Ax\frac{\partial}{\partial y}(\delta\Sigma) + \Sigma_0\left(\frac{\partial v_x}{\partial x} + \frac{\partial v_y}{\partial y}\right) = 0 \tag{2.5}$$

$$\left(\frac{\partial^2}{\partial x^2} + \frac{\partial^2}{\partial y^2} + \frac{\partial^2}{\partial z^2}\right)(\delta\Phi) = 4\pi G\delta\Sigma\delta(z) \tag{2.6}$$

The differential rotation of the galactic disc introduces shear in the system. To account for this, a sheared coordinate system is introduced.

Sheared coordinate system: In a differentially rotating galactic disc, each circular layer of the disc rotates with a slightly different angular speed. As a result, fluid elements located at different radial positions drift in the azimuthal direction. Due to this drift, a local linear shear is created, where the background velocity varies only with radius but is directed entirely along the azimuthal axis. To examine small perturbations in such a differential rotating system, it is useful to adopt the *sheared coordinate system*, which coincides with the background shear flow. In this approach, the radial coordinate remains unchanged, while the azimuthal coordinate is shifted by an amount proportional to time and radial position. The transformation is typically written as

$$x' = x, \qquad y' = y - 2Axt, \qquad z' = z, \qquad t' = t \tag{2.7}$$

This coordinate system removes the continuous sideways drift seen in the standard (x, y) frame, making the unperturbed flow appear stationary. As a result, the governing equations for density, velocity, and potential perturbations become simpler. The sheared coordinates also naturally capture the time-dependent evolution of wave modes, particularly the change in radial wavenumber that plays a very important role in the swing amplification of spiral arms.

Under the above coordinate transformation, the spatial and temporal derivatives can be written as

$$\frac{\partial}{\partial x} = \frac{\partial}{\partial x'} - 2At'\frac{\partial}{\partial y'} \tag{2.8}$$

$$\frac{\partial}{\partial y} = \frac{\partial}{\partial y'} \tag{2.9}$$

$$\frac{\partial}{\partial z} = \frac{\partial}{\partial z'} \tag{2.10}$$

$$\frac{\partial}{\partial t} = \frac{\partial}{\partial t'} - 2Ax'\frac{\partial}{\partial y'} \tag{2.11}$$

Also, in the sheared frame τ is introduced, which is a dimension less measurement of time in sheared cordinate (t').

$$\tau = 2At' - \frac{k_x}{k_y} \tag{2.12}$$

τ has different zeros for every mode with a different value of $\frac{k_x}{k_y}$.
When $\tau = 0$,

$$\exp\left[i\left(k_x x' + k_y y'\right)\right] = \exp\left[i\left(k_y(\tau x + y)\right)\right] \tag{2.13}$$

Thus the local, linearized perturbation equations (Eqs. 2.3 - 2.6) can be written in term of the sheared coordinate system using (Eqs. 2.7 - 2.11)

$$\frac{\partial v_x}{\partial \tau} - \frac{\Omega}{A} v_y = -i \frac{k_y}{2A} \tau \left[-\delta\Phi - \frac{c^2}{\Sigma_0} (\delta\Sigma) \right]. \tag{2.14}$$

$$\frac{\partial v_y}{\partial \tau} + \frac{B}{A} v_x = i \frac{k_y}{2A} \left[-\delta\Phi - \frac{c^2}{\Sigma_0} (\delta\Sigma) \right]. \tag{2.15}$$

$$\frac{\partial}{\partial \tau} (\delta\Sigma) - i \frac{k_y}{2A} \tau \Sigma_0 v_x + i \frac{k_y}{2A} \Sigma_0 v_y = 0. \tag{2.16}$$

$$\left[-k_y^2 (1 + \tau^2) - \frac{\partial^2}{\partial z^2} \right] (\delta\Phi) = 4\pi G \Sigma \, \delta\Sigma \, \delta(z'). \tag{2.17}$$

In the sheared coordinate system, the wavenumber is constant; however, in the uniformly rotating frame, the wavenumber increases with τ, where $k_{\text{non-sheared}} = k_y(1 + \tau^2)$ (Chanda J. Jog, 1992). The solution of the perturbed potential equation 2.17 is given by

$$\delta\Phi = \left[-\frac{2\pi G}{k_y (1 + \tau^2)^{1/2}} \right] (\delta\Sigma). \tag{2.18}$$

Next define θ_i, the dimensionless perturbed surface density which is the ratio of the perturbed surface density to the unperturbed surface density.

$$\theta_i = \frac{\delta\Sigma}{\Sigma} \tag{2.19}$$

Finite thickness of the galactic disc is introduced into the formulation as follows: For simplicity, the density of the galactic disc is assumed to be constant (i.e., it does not vary with the scale height z). Due to the finite thickness of the disc, a reduction in the radial force is observed in the mid-plane ($z = 0$) by a factor of $\frac{1-e^{-kh}}{kh}$ along the axisymmetric case (Toomre, 1964; Chanda J Jog and Solomon, 1984; Chanda J. Jog, 2014).

Similarly, for the non-axisymmetric case, due to the finite thickness of the galactic disc, a reduction in the perturbed force is observed by a factor of δ along in the direction of x' and y' in the shear frame.

$$\delta = \frac{1 - \exp\left[-k_y (1 + \tau^2)^{1/2} h \right]}{k_y (1 + \tau^2)^{1/2} h}. \tag{2.20}$$

where δ is the reduction factor.

After solving the local, linearised perturbed Euler equations, Poisson equation and equation of continuity (Goldreich and Lynden-Bell, 1965), the reduction factor only modifies the self-gravity term and the resultant equation is given as (Ghosh and Chanda J Jog, 2018):

$$\begin{aligned} \left(\frac{d^2\theta}{d\tau^2} \right) - \left(\frac{d\theta}{d\tau} \right) \left(\frac{2\tau}{1 + \tau^2} \right) + \theta \Bigg[& \frac{\kappa^2}{4A^2} + \frac{2B/A}{1 + \tau^2} + \frac{k_y^2 c^2}{4A^2} (1 + \tau^2) \\ & - \Sigma \left(\frac{\pi G k_y}{2A^2} \right) (1 + \tau^2)^{1/2} \frac{1 - \exp[-k_y (1 + \tau^2)^{1/2} h]}{k_y (1 + \tau^2)^{1/2} h} \Bigg] = 0 \end{aligned} \tag{2.21}$$

The first term in the Eq. 2.21 describes the acceleration of the perturbation with respect to the dimensionless time variable τ, while the second term indicates the rate at which the perturbation evolves. The four terms enclosed within the square brackets of Eq. 2.21 correspond to the epicyclic motion, the background shear flow, the pressure of the disc material, and the self-gravity of the disc, which is further influenced by its finite thickness. For small values of τ, the self-gravity dominate over pressure, and for large values of $|\tau|$, the pressure term becomes dominant over the other terms, resulting in a solution that is oscillatory in nature.

We define maximum amplification factor (MAF) for a given mode as follows:

$$\mathrm{MAF} = \frac{\theta_{\max}}{\theta_{ini}}$$

where $\theta_{\max}$ is the maximum amplitude of oscillation and θ_{ini} is the initial amplitude of oscillation (as shown in 2.1).

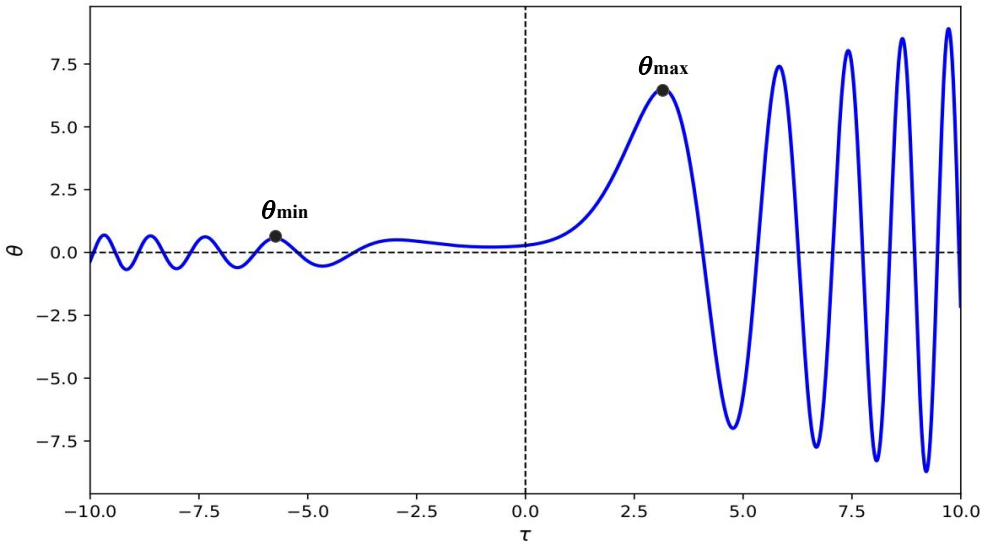


Figure 2.1: Evolution of θ, the ratio of the perturbed to unperturbed surface density, as a function of the dimensionless time τ in the sheared frame. The perturbation begins in a leading configuration ($\tau < 0$) and is transformed into a trailing one ($\tau > 0$) by the differential rotation of the disc. The point $\tau \approx 0$ corresponds to the leading-to-trailing transition, during which swing amplification reaches at its maximum value.

We now introduce three dimensionless parameters, namely the Toomre Q parameter defined as $Q = \kappa c/(\pi G\Sigma)$, the shear parameter $\eta = 2A/\Omega$, and the dimensionless radial wavenumber $X = k_y/k_{\mathrm{crit}}$, where $k_{\mathrm{crit}} = \kappa^2/(2\pi G\Sigma)$. We further define the dimensionless vertical wavenumber as $k_y h = (k_y/k_{\mathrm{crit}})(k_{\mathrm{crit}}h) = X^{-1}\beta$, where $\beta = k_{\mathrm{crit}}h$.

Equation (2.21) can then be expressed in terms of these quantities, which yields the evolution of θ as a function of τ:

$$\left(\frac{d^2\theta}{d\tau^2}\right) - \left(\frac{d\theta}{d\tau}\right)\left(\frac{2\tau}{1+\tau^2}\right) + \theta\Bigg[\xi^2 + \frac{2(\eta-2)}{\eta(1+\tau^2)} + \frac{(1+\tau^2)Q^2\xi^2}{4X^2} - \frac{\xi^2}{X}(1+\tau^2)^{1/2}\frac{1-\exp[-X^{-1}\beta(1+\tau^2)^{1/2}]}{X^{-1}\beta(1+\tau^2)^{1/2}}\Bigg] = 0 \tag{2.22}$$

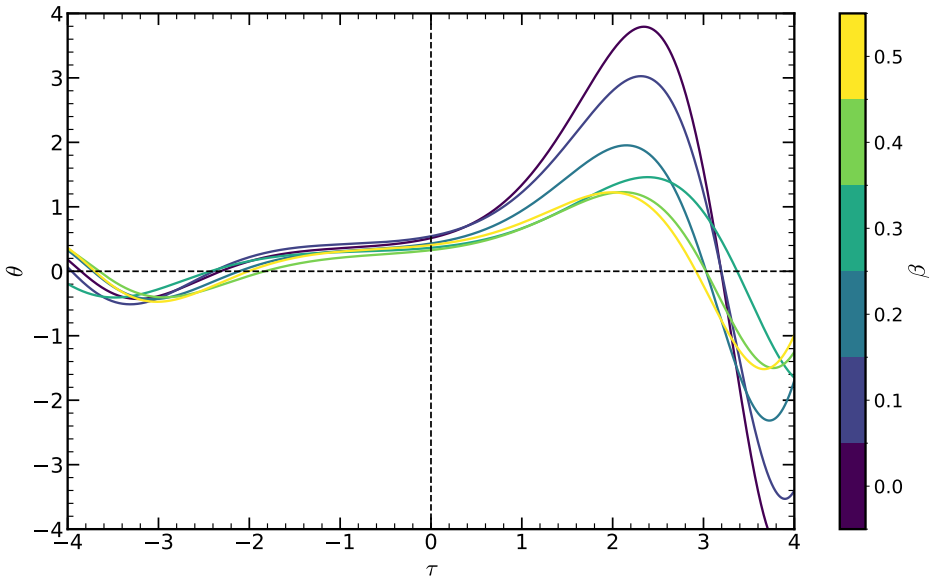


Figure 2.2: Evolution of θ, the ratio of the perturbed to unperturbed surface density, as a function of the dimensionless time (τ), in the sheared frame with different galactic disc height β (0.0, 0.1, 0.2, 0.3, 0.4, 0.5) for Toomre stability factor $Q = 1.3$, $X = 1$, $\eta = 1$, respectively. The maximum amplification factor (MAF) decreases with an increase in the disc thickness.

where $\xi^2 = \kappa^2/(4A^2) = 2(2-\eta)/\eta^2$.

Figure 2.2 shows the evolution of the perturbation in surface density of galactic disc θ, defined as the ratio of the perturbed to the unperturbed surface density, plotted as a function of the dimensionless time τ in a shearing galactic disk. Each coloured curve represents a different value of the disc scale height β, ranging from 0.0 to 0.5 (from infinitesimal zero to thick disc). The results are computed for a constant Toomre stability parameter $Q = 1.3$, $X = 1$, and shear parameter $\eta = 1$, corresponding to a one-fluid galactic disc. For $\tau < 0$, the perturbation remains weak while it is in the leading configuration. As it swings from leading to trailing $\tau = 0$, self-gravity amplifies the perturbation, producing a peak known as the maximum amplification factor (MAF). The plot clearly shows that increasing disk thickness (larger β) reduces the peak amplitude of swing amplified spiral arm also signifies that disc thickness weakens the self-gravity and suppresses the swing amplification.

If $\beta \to 0$, the equation reduces to the case of an infinitesimally thin disc (Chanda J. Jog, 1992).

$$\left(\frac{d^2\theta}{d\tau^2}\right) - \left(\frac{d\theta}{d\tau}\right)\left(\frac{2\tau}{1+\tau^2}\right) + \theta\left[\xi^2 + \frac{2(\eta-2)}{\eta(1+\tau^2)} + \frac{(1+\tau^2)Q^2\xi^2}{4X^2} - \frac{\xi^2}{X}(1+\tau^2)^{1/2}\right] = 0 \tag{2.23}$$

The equation reduces standard equation for an infinitesimally thin disc.

Now the Eq. 2.21 can be solved using numerical analysis by the fourth-order Runga-Kutta method by using canonical boundary conditions (0,1), (1,0), which reduced this equation into two coupled first-order linear differential equations θ, $\frac{d\theta}{d\tau}$. The value of MAF depends very sensitively on the choice of $\tau_{\rm ini}$. The value of $\tau_{\rm ini}$ is optimised in such a way that the MAF would be the maximum. In this one fluid case, value of $\tau_{\rm ini}$ is -25.

2.1.1 Numerical Solution

Evolution of non-axisymmetric perturbations in one-fluid galactic disc is governed by second-order linear differential equations of variable (θ_s . For numerical solution, this equation are written as a system of two first-order differential equations in the variables θ_s and $d\theta_s/d\tau$. This formulation allows the use of the fourth-order Runge–Kutta (RK4) method, which is the method for integrating the system over the dimensionless time variable τ (Chanda J. Jog, 1992). The system is solved by applying canonical initial conditions. For the one-fluid case, the canonical condition $(1, 0)$ is imposed at the initial integration time, $\tau = \tau_{\rm ini}$. Since the physical initial state of perturbations in a galactic disc is not uniquely specified, two possible initial configurations (1,0) and (0,1) are considered. For best initial configuration, the numerical integration is repeated for different choices of $\tau_{\rm ini}$.

It is important to note that the *maximum amplification factor* (MAF) obtained from the integration is *highly sensitive* to the value of $\tau_{\rm ini}$. Therefore, $\tau_{\rm ini}$ is treated as an optimisation parameter, and the value of $\tau_{\rm ini}$ that yields the largest MAF is selected (Toomre, 1981). The numerical procedure consists of:

1. Converting the second-order equations into a system of first-order differential equations,
2. Applying canonical initial conditions at $\tau = \tau_{\rm ini}$, $\tau_{\rm ini}$ = -25
3. Integrating the system using the RK4 method,
4. Select the solution corresponding to the maximum amplification factor (MAF), representing the represent the amplified spiral mode.

2.2 Two-fluid galactic disc with finite thickness

In this section, the galactic disc is modelled as a gravitationally coupled system consisting of both stars and gas that corotate with each other. Each component is treated as isothermal fluid and is characterised by its surface density Σ_i, one-dimensional velocity dispersion, or equivalently the sound speed c_i, where $i = s, g$ denote the stars and gas, respectively. Observational studies of galaxies in the local universe show that the stellar velocity dispersion is typically higher than that of the gas, and this assumption is used here.

Local perturbations characterised by wavelengths smaller than the galactocentric radial distance are analysed. The perturbations are assumed to be planar, and the length of the perturbation is greater than the scale height of the disc. In the mathematical framework, i=s and i=g describe the equation for star and gas, respectively.

The general form of the Euler equation governing fluid motion can be written as

$$\frac{\partial \mathbf{V}}{\partial t} + (\mathbf{V} \cdot \nabla)\mathbf{V} = -\frac{1}{\rho}\nabla P - \nabla\Phi \tag{2.24}$$

The galactic disc undergoes differential rotation; therefore, the fluid equations (stars and gas) are most conveniently expressed in a rotating reference frame, where the Euler equation modified by the presence of coriolis and centrifugal force

$$\frac{\partial \mathbf{V}_i}{\partial t} + (\mathbf{V}_i \cdot \nabla)\mathbf{V}_i = -\frac{c_i^2}{\Sigma_{0i}}\nabla\Sigma_i - \nabla(\Phi_i) - 2\boldsymbol{\Omega} \times \mathbf{V}_i + \boldsymbol{\Omega}^2\mathbf{r} \tag{2.25}$$

In this formulation of rotating galactic disc, the quantity $\mathbf{V}_i$ represents the two-dimensional velocity of the i-th fluid component with respect to the rotating axes, c_i is the sound speed (or velocity dispersion) and μ_{0i} is the unperturbed surface density. A Cartesian coordinate system (x, y, z) is defined with its center at (R_0, ϕ_0), and unit vectors $\hat{i}, \hat{j}, \hat{k}$ such that $\hat{i}$ coincides with the initial outward radial direction. The non-axisymmetric perturbation analysis is then carried out within this local region. The local, linear perturbed Euler equation in Cartesian coordinates is given by

$$\frac{\partial v_{xi}}{\partial t} + 2Ax\frac{\partial v_{xi}}{\partial y} - 2\Omega v_{yi} = -\frac{\partial}{\partial x}(\delta\phi_i) - \frac{c_i^2}{\Sigma_{0i}}\frac{\partial(\delta\Sigma_i)}{\partial x} \tag{2.26}$$

$$\frac{\partial v_{yi}}{\partial t} + 2Ax\frac{\partial v_{yi}}{\partial y} - 2Bv_{xi} = -\frac{\partial}{\partial x}(\delta\phi_i) - \frac{c_i^2}{\Sigma_{0i}}\frac{\partial(\delta\Sigma_i)}{\partial x} \tag{2.27}$$

The linear perturbation equations corresponding to the continuity and Poisson equations are given by

$$\frac{\partial(\delta\Sigma_i)}{\partial t} + 2Ax\frac{\partial(\delta\Sigma_i)}{\partial y} + \Sigma_{0i}\left(\frac{\partial v_{xi}}{\partial x} + \frac{\partial v_{yi}}{\partial y}\right) = 0 \tag{2.28}$$

$$\left(\frac{\partial^2}{\partial x^2} + \frac{\partial^2}{\partial y^2} + \frac{\partial^2}{\partial z^2}\right)(\delta\phi_i) = 4\pi G(\delta\Sigma_i + \delta\Sigma_g)\delta(z) \tag{2.29}$$

where, $\delta\phi_i = (\delta\phi_s + \delta\phi_g)$ is the total perturbed gravitational potential, Σ_{0i} and $\delta\Sigma_i$ are the unperturbed and perturbed surface densities for the i^{th} component.

Thus the local, linearized perturbation (Eqs. 2.26 - 2.29) can be written in term of the sheared coordinate system using (Eqs. 2.7 - 2.11)

$$\frac{\partial v_{xi}}{\partial \tau} - \frac{\Omega}{A}v_{yi} = -i\frac{k_y}{2A}\tau\left[-(\delta\phi_s + \delta\phi_g) - \frac{c_i^2}{\Sigma_{0i}}(\delta\Sigma_i)\right] \tag{2.30}$$

$$\frac{\partial v_{yi}}{\partial \tau} + \frac{B}{A}v_{xi} = i\frac{k_y}{2A}\left[-(\delta\phi_s + \delta\phi_g) - \frac{c_i^2}{\Sigma_{0i}}(\delta\Sigma_i)\right] \tag{2.31}$$

$$\frac{\partial}{\partial \tau}(\delta\Sigma_i) - i\frac{k_y}{2A}\tau\Sigma_{0i}v_{xi} + i\frac{k_y}{2A}\Sigma_{0i}v_{yi} = 0 \tag{2.32}$$

$$\left[-k_y^2(1+\tau^2) + \frac{\partial^2}{\partial z^2}\right](\delta\phi_s + \delta\phi_g) = 4\pi G(\delta\Sigma_s + \delta\Sigma_g)\delta(z') \tag{2.33}$$

Let us consider

$$-k_y^2(1+\tau^2) = k$$

$$\theta_i = \frac{\delta\Sigma_i}{\Sigma_{0i}} \tag{2.34}$$

$$\frac{d^2\theta_i}{d\tau^2} - \left(\frac{d\theta_i}{d\tau}\right)\left(\frac{2\tau}{1+\tau^2}\right) + \theta_i\left[\frac{\kappa^2}{4A^2} + \frac{2B/A}{1+\tau^2} + \frac{k_y^2}{4A^2}(1+\tau^2)c_i^2\right]$$
$$= (\Sigma_{0s}\theta_s + \Sigma_{0g}\theta_g)\left(\frac{\pi G k_y}{2A^2}\right)(1+\tau^2)^{1/2} \tag{2.35}$$

The evolution of the system is governed by the interplay of shear rate, epicyclic motion, pressure and self gravity. For large τ, pressure dominates and the solution is oscillatory, with a frequency set by the velocity dispersion. Near less value of τ, epicyclic and shear terms cancel out, which allows the gravitational term to dominate, causing the transient swing amplification phenomenon: a temporary amplification of θ_i as the perturbation swings from leading to trailing. After the swing amplification, the pressure term again dominates, restoring oscillatory behaviour. This is essential for understanding how spiral arms are dynamically amplified within disc galaxies.

We now introduce five dimensionless parameters which define as

$$Q_s = \frac{\kappa c_s}{\pi G \mu_{0s}}, \qquad Q_g = \frac{\kappa c_g}{\pi G \mu_{0g}}, \qquad \epsilon = \frac{\mu_{0g}}{\mu_{0g} + \mu_{0s}}, \qquad \eta = \frac{2A}{\Omega_0}, \qquad X = \frac{\lambda_y}{\lambda_{\rm crit}}. \tag{2.36}$$

Q_s, Q_g are the stability factor (Toomre Q-factor) along axisymmetric(Toomre, 1964), ϵ is the gas mass fraction, η is the logarithmic shear rate and X is the wavelength of perturbation.

Eq.2.35 can then be expressed in terms of these quantities, which yields the evolution of θ as a function of τ:

$$\left(\frac{d^2\theta_s}{d\tau^2}\right) - \left(\frac{d\theta_s}{d\tau}\right)\left(\frac{2\tau}{1+\tau^2}\right) + \theta_s\left[\xi^2 + \frac{2(\eta-2)}{\eta(1+\tau^2)} + \frac{(1+\tau^2)Q_s^2(1-\epsilon)^2\xi^2}{4X^2}\right] = \frac{\xi^2}{X}(1+\tau^2)^{1/2}\left[\theta_s(1-\epsilon) + \theta_g\epsilon\right], \tag{2.37}$$

$$\left(\frac{d^2\theta_g}{d\tau^2}\right) - \left(\frac{d\theta_g}{d\tau}\right)\left(\frac{2\tau}{1+\tau^2}\right) + \theta_g\left[\xi^2 + \frac{2(\eta-2)}{\eta(1+\tau^2)} + \frac{(1+\tau^2)Q_g^2\epsilon^2\xi^2}{4X^2}\right] = \frac{\xi^2}{X}(1+\tau^2)^{1/2}\left[\theta_s(1-\epsilon) + \theta_g\epsilon\right]. \tag{2.38}$$

Here, we adopt a more realistic modelling of a galactic disc, each fluid component is assumed to have a finite vertical thickness $2h_i$, where $i = s, g$ denotes the stellar and gaseous components, respectively. The effect of vertical thickness leads to a reduction in the perturbed gravitational force appearing in the Euler equation formulated in the sheared frame. This reduction can be quantified by a thickness reduction factor δ_i for each component, which is given by

$$\delta_i = \frac{1 - e^{-kh_i}}{kh_i}, \tag{2.39}$$

where k is the radial wavenumber of the perturbation.

Stars and gas are considered as the isothermal fluids, and each of the fluids has a total thickness of 2h. In a similar way reduction factor δ_i is introduced:

$$\delta_i = \frac{1 - \exp\left[-k_y(1+\tau^2)^{1/2}h_i\right]}{k_y(1+\tau^2)^{1/2}h_i}. \tag{2.40}$$

The solution of the perturbed Euler equation (Ghosh and Chanda J Jog, 2018):

$$\frac{d^2\theta_i}{d\tau^2} - \left(\frac{d\theta_i}{d\tau}\right)\left(\frac{2\tau}{1+\tau^2}\right) + \theta_i\left[\frac{\kappa^2}{4A^2} + \frac{2B/A}{1+\tau^2} + \frac{k_y^2 c_i^2}{4A^2}(1+\tau^2)\right] = \frac{\pi G k_y}{2A^2}(1+\tau^2)^{1/2}\sum_i \delta_{\Sigma_i}\frac{1-\exp\left[-k_y(1+\tau^2)^{1/2}h_i\right]}{k_y(1+\tau^2)^{1/2}h_i}. \tag{2.41}$$

Solution of equation 2.41 in dimensionless parameter: For stars

$$\left(\frac{d^2\theta_s}{d\tau^2}\right) - \left(\frac{d\theta_s}{d\tau}\right)\left(\frac{2\tau}{1+\tau^2}\right) + \theta_s\left[\xi^2 + \frac{2(\eta-2)}{\eta(1+\tau^2)} + \frac{(1+\tau^2)Q_s^2(1-\epsilon)\xi^2}{4X^2}\right] = \frac{\xi^2}{X}(1+\tau^2)^{1/2}\left[\theta_s(1-\epsilon)\frac{1-\exp\left(-X^{-1}\beta_s(1+\tau^2)^{1/2}\right)}{X^{-1}\beta_s(1+\tau^2)^{1/2}} + \theta_g\epsilon\frac{1-\exp\left(-X^{-1}\beta_g(1+\tau^2)^{1/2}\right)}{X^{-1}\beta_g(1+\tau^2)^{1/2}}\right]. \tag{2.42}$$

For gas:

$$\left(\frac{d^2\theta_g}{d\tau^2}\right) - \left(\frac{d\theta_g}{d\tau}\right)\left(\frac{2\tau}{1+\tau^2}\right) + \theta_g\left[\xi^2 + \frac{2(\eta-2)}{\eta(1+\tau^2)} + \frac{(1+\tau^2)Q_g^2\epsilon^2\xi^2}{4X^2}\right] = \frac{\xi^2}{X}(1+\tau^2)^{1/2}\left[\theta_s(1-\epsilon)\frac{1-\exp\left(-X^{-1}\beta_s(1+\tau^2)^{1/2}\right)}{X^{-1}\beta_s(1+\tau^2)^{1/2}} + \theta_g\epsilon\frac{1-\exp\left(-X^{-1}\beta_g(1+\tau^2)^{1/2}\right)}{X^{-1}\beta_g(1+\tau^2)^{1/2}}\right]. \tag{2.43}$$

Figure 2.3 shows the temporal evolution of the dimensionless perturbation amplitude, θ, for both the stellar and gaseous components. The stellar component, represented by the black curve, remains weakly oscillatory over the entire range of τ, with only modest amplification near $\tau \sim 3$. In contrast, the gaseous component, shown by the orange curve, exhibits a much stronger response. For $\tau < 0$, both components display relatively small oscillations, indicating weak leading perturbations. As the perturbation passes through $\tau = 0$, corresponding to the transition from leading to trailing configurations, the gas component begins to grow rapidly.

A prominent amplification peak appears around $\tau \sim 3$, where the gaseous response becomes significantly larger than the stellar response. After this peak, the gas amplitude decreases sharply and becomes negative, followed by another rapid increase at larger τ. This strong behaviour of the gas component arises because the lower value of $Q_{\rm g} = 1.2$ makes the gaseous disk more susceptible to self-gravity and swing amplification. On the other hand, the higher stellar Toomre parameter, $Q_{\rm s} = 1.8$, indicates a more stable stellar disk, suppressing large-scale amplification. Therefore, the figure demonstrates that gas plays a dominant role in enhancing non-axisymmetric perturbations in the disk compared to stars.

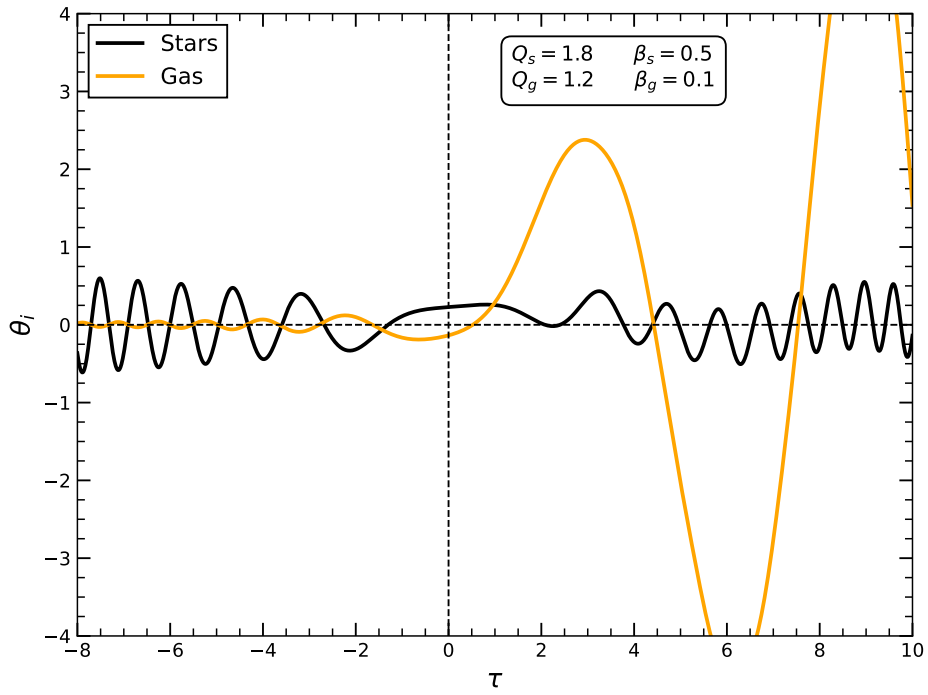


Figure 2.3: Evolution of θ, the ratio of the perturbed to unperturbed surface density, as a function of the dimensionless time (τ), for the stellar and gaseous components in a two-fluid galactic disc. The black curve corresponds to the stellar component with $Q_{\rm s} = 1.8$ and $\beta_{\rm s} = 0.5$, while the orange curve represents the gaseous component with $Q_{\rm g} = 1.2$ and $\beta_{\rm g} = 0.1$.

Evolution of non-axisymmetric perturbations in two-fluid galactic disc (stars and gas) is governed by two coupled, second-order linear differential equations (θ_s and θ_g). For numerical solution, these coupled equations are written as a system of four first-order differential equations in the variables θ_s, $d\theta_s/d\tau$, θ_g, and $d\theta_g/d\tau$ while for one fluid galactic disc (stellar) is governed by second-order linear differential equation in the variable θ and for numerical solution, this equation as two first-order differential equation in the variables θ and $d\theta/d\tau$. This formulation allows the use of the fourth-order Runge–Kutta (RK4) method, which is the method for integrating the system over the dimensionless time variable τ (Chanda J. Jog, 1992). The system is solved by applying canonical boundary conditions. For the two-fluid galactic disc, the conditions are specified as $(1, 0, 0, 0)$, while for the one-fluid case, the canonical condition $(1, 0)$ is imposed at the initial integration time, $\tau = \tau_{\rm ini}$. Since the physical initial state of perturbations in a galactic disc is not uniquely specified, several possible initial configurations are considered, corresponding to perturbations initially dominated by either the stellar component, the gaseous component, or mixed combinations of the two. For each initial configuration, the numerical integration is repeated for different choices of $\tau_{\rm ini}$. It is important to note that the *maximum amplification factor* (MAF) obtained from the integration is *highly sensitive* to the value of $\tau_{\rm ini}$. Therefore, $\tau_{\rm ini}$ is treated as an optimisation parameter, and the value of $\tau_{\rm ini}$ that yields the largest MAF is selected (Toomre, 1981).

The numerical procedure consists of:

1. Converting the second-order equations into a system of first-order differential equations,

2. Applying canonical initial conditions at $\tau = \tau_{ini}$, τ_{ini} = -25
3. Integrating the system using the RK4 method,
4. Select the solution corresponding to the maximum amplification factor (MAF), representing the represent the amplified spiral mode.

Chapter 3

Results

3.1 *Variation of swing-amplified spirals with shear rate for One fluid case*

In this section we represents the variation of maximum amplification factor and pitch angle of swing amplified spirals with shear rate for varying parameters e.g. disc scale height (β), Toomre stability factor (Q) and X.

3.1.1 *Variation of MAF with shear rate*

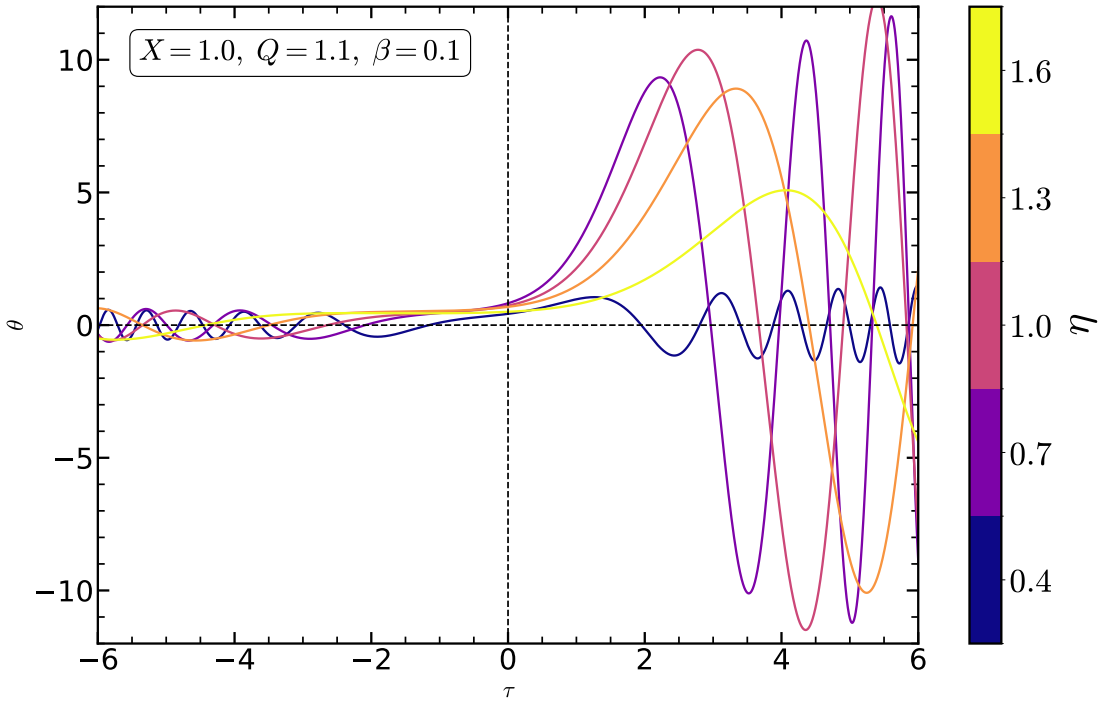


Figure 3.1: The temporal evolution of $\theta = \delta\Sigma/\Sigma$, the ratio of the perturbed to unperturbed surface density, as a function of the dimensionless time (τ), in the sheared frame with different shear rate (η) (see the colour bar) with parameter fixed at $Q = 1.1$, $\beta = 0.1$, $X = 1$.

In Figure 3.1 negative values of τ correspond to the leading mode of the perturbation, while positive values correspond to the trailing mode. Perturbation undergoes significant amplification as it evolves from the leading mode to the trailing mode. The behavior of θ with τ is obtained by considering the evolution of a mode from a leading mode ($\tau < 0$, $|\tau|$ large), through a radial configuration ($\tau \sim 0$), to a trailing mode ($\tau > 0$, $|\tau|$ large). At large $|\tau|$, the pressure term dominates, and the solution for θ is oscillatory with almost the constant amplitude for both ($\tau < 0$) and ($\tau > 0$). As the mode evolves from a leading to a radial configuration ($\tau \sim 0$), the terms associated with epicyclic motion and shear become very significant, and they nearly cancel each other. Thus, these two effects are in approximate resonance for realistic rotation laws, with the cancellation becoming exact for a flat rotation curve. Swing amplification is possible only when self gravity

dominates pressure term. In this case, θ get significantly increases as it evolves from radial ($\tau = 0$) to trailing mode ($\tau > 0$), peak amplitude is referred to as the Maximum Amplification Factor (MAF), which characterizes the strength of swing amplification. The swing amplification is temporary. At sufficiently large $\tau > 0$, the pressure term again becomes dominant and the solution returns to an oscillatory form, provided that the system remains in the linear regime at all times.

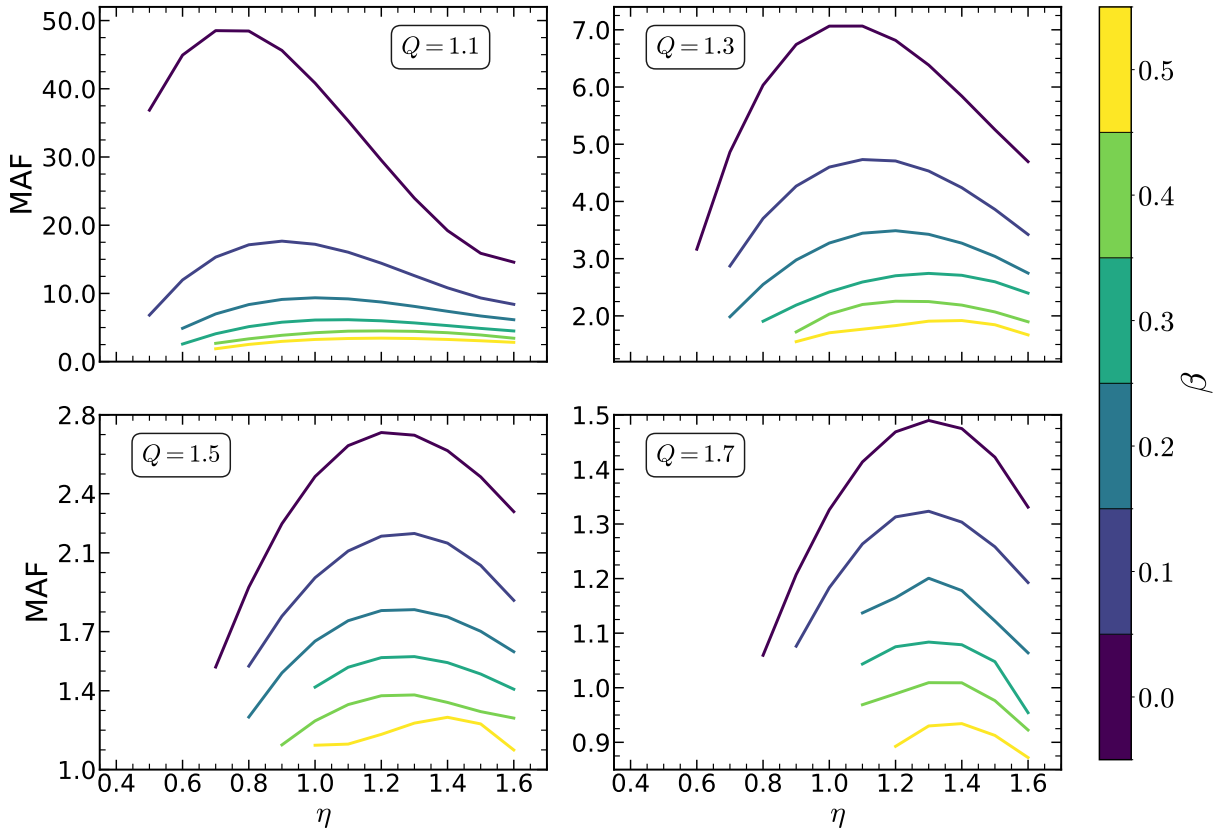


Figure 3.2: Systematic variation of the Maximum Amplification Factor (MAF) with the shear rate (η) for swing amplified spiral arms, for different disc scale height (β) and for different values of Toomre Q parameter. For given Q value, and for a fixed β, the MAF tends to attain its maximum around $\eta \sim 1$. This trend holds true for almost the entire parameter regime considered here.

We examined the variation of MAF with shear rate with the inclusion of finite thickness. We took the different values of Q (see Figure 3.2) to check the effect of perturbation on stable galactic disc. The main findings are

- The resulting maximum amplification factor (MAF) of the swing-amplified spiral structure decreases monotonically with increasing disc thickness, indicating that finite thickness weakens the self-gravity of the disc.
- For a fixed disc thickness, the MAF decreases with increasing Toomre stability factor Q, implying that more stable discs are less efficient at supporting swing amplification.
- The reduction in MAF due to finite disc thickness is more pronounced at lower values of Q, whereas for larger Q the amplification is already weak and the effect of thickness becomes less significant.

The observed trends can be understood from the combined effects of shear, disc thickness, and gravitational stability. Shear plays a crucial role in swing amplification because it determines how efficiently leading perturbations are transformed into trailing spiral features. When the shear is very weak, the differential rotation is insufficient to stretch and amplify the perturbation effectively. On the other hand, when the shear is too strong, the perturbation is rapidly wound up and dispersed before significant amplification can occur. As a result, spiral amplification is strongest only within an intermediate range of shear.

The finite thickness of the disc also has an important effect on the amplification process. In a thin disc, most of the mass is concentrated close to the mid-plane, producing a stronger in-plane gravitational force. This stronger self-gravity allows density perturbations to grow more efficiently and leads to larger amplification factors. As the disc thickness increases, the mass becomes distributed over a larger vertical extent, reducing the in-plane self-gravity. Consequently, the ability of the disc to support and amplify spiral perturbations becomes weaker, leading to a systematic decrease in the maximum amplification factor.

The Toomre stability factor further regulates the growth of spiral structure. Lower values of Q correspond to colder discs with lower random motions, where self-gravity dominates over pressure support and perturbations can grow efficiently. In contrast, larger values of Q represent dynamically hotter and more stable discs, in which random motions suppress the growth of non-axisymmetric perturbations. Therefore, the maximum amplification factor decreases steadily with increasing Q.

Overall, the strongest swing amplification occurs in relatively thin discs with moderate shear, whereas thick, high Q discs exhibit much weaker spiral growth.

3.1.2 *Variation of pitch angle with shear rate*

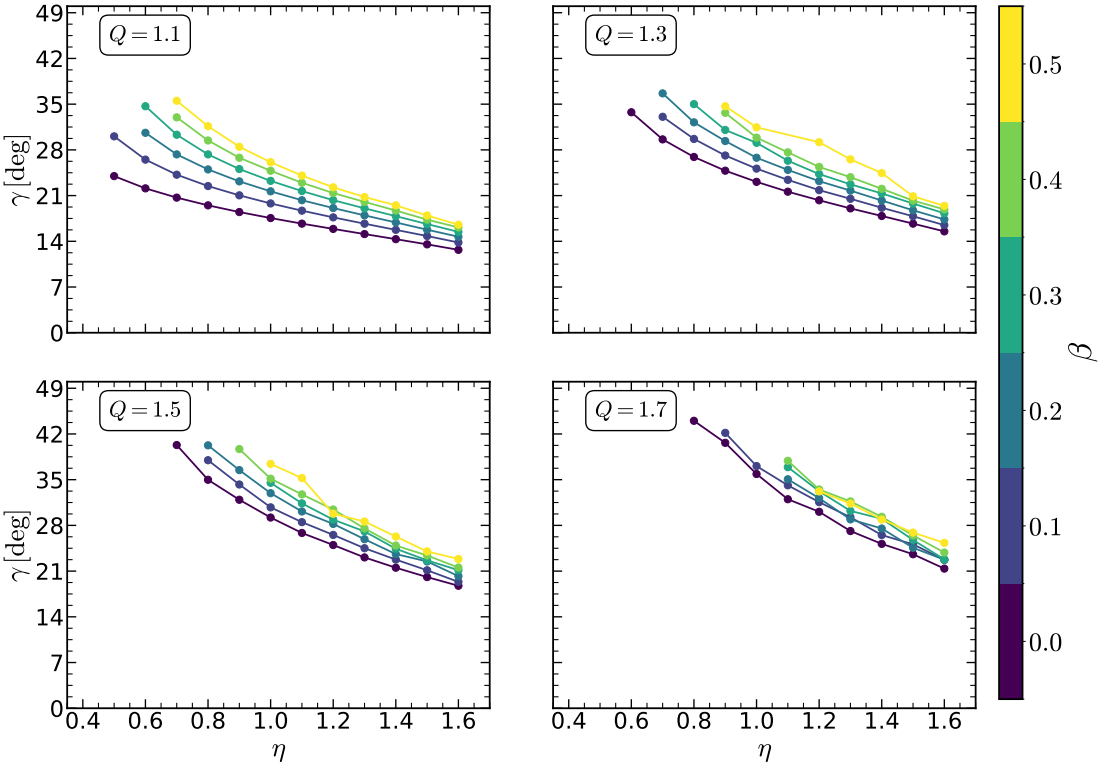


Figure 3.3: Systematic variation of the pitch angle (γ) with the shear rate (η) for swing amplified spiral arms, for different disc scale height (β) and for different value of Toomre Q parameter at wavelength parameter X = 1.

We examined the variation of pitch angle with shear rate with the inclusion of finite thickness. We took the different values of Q (see Figure 3.3) to check the effect of perturbation on stable galactic disc. The main finding are

- The pitch angle decreases monotonically with increasing shear rate for all values of disc thickness, indicating that stronger differential rotation produces more tightly wound spiral arms.
- For a fixed shear rate, the pitch angle increases with increasing disc thickness, implying that finite thickness leads to relatively more open spiral structures.
- The effect of finite disc thickness on the pitch angle is more significant at lower values of the Toomre stability factor Q, whereas for larger Q the differences in pitch angle between discs of different thickness become smaller.

For all values of the disc scale height β, the pitch angle decreases monotonically with increasing shear rate, indicating that stronger differential rotation produces more tightly wound spiral arm structures. The same overall trend is observed for different values of the Toomre stability parameter, Q. The inclusion of finite disc thickness systematically increases the pitch angle. At a fixed shear rate, a larger value of β results in a larger pitch angle, implying that thicker discs tend to support more loosely wound spiral structures. The Toomre stability parameter, Q, quantifies the stability of the disc against axisymmetric gravitational perturbations. A larger value of Q corresponds to a

more stable disc, since the random motions of stars dominate over the disc self-gravity. In contrast, a lower value of Q indicates that self-gravity is relatively stronger and can effectively amplify perturbations. At low values of the shear rate, η, the differential rotation is weak, and the amplification of spiral features depends primarily on the strength of self-gravity. Consequently, swing amplification is generally suppressed at low shear rates. When the Toomre parameter is small, the stronger self-gravity can still amplify the perturbation and allow swing amplification to occur. However, for larger values of Q, the disc becomes sufficiently stable that self-gravity is too weak to drive the growth of perturbations. In such cases, the weak differential rotation at low η is insufficient to produce swing amplification. Therefore, discs with high Q do not exhibit swing-amplified spiral structures at low shear rates because the combined effects of weak shear and reduced self-gravity prevent the perturbations from growing.

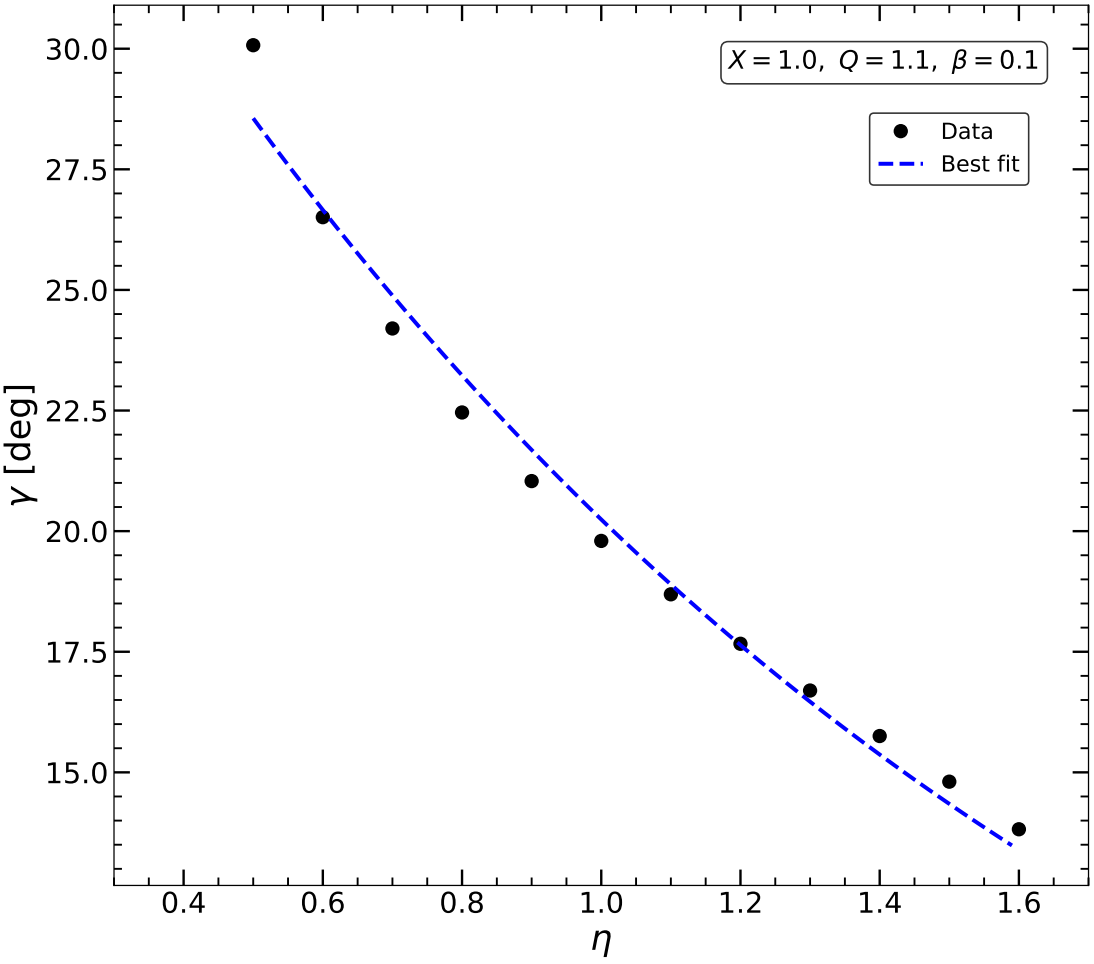


Figure 3.4: Pitch angle (γ) as a function of the shear rate η for $Q = 1.1$, $\beta = 0.1$, and $X = 1.0$. The blue markers denote the numerical results obtained from the swing amplification calculations. The solid orange curve represents the best exponential fit to the data, $\gamma = A\exp(-B(\eta - \eta_0)$, where the η_0 is 0.4, with the fitted parameters $A = 30.5929 \pm 0.5303$ and $B = 0.6883 \pm 0.029$.

$$\gamma = A\, e^{-B(\eta-\eta_0)}$$

where γ is the pitch angle, η is the shear rate, η_0 is also shear which is taken as 0.4 a

and b are the fitting parameter.

$$\frac{d\gamma}{d\eta} = -ABe^{-b(\eta-\eta_0)}$$

$$\frac{d\gamma}{d\eta} = -B\gamma$$

$$B = \left|\frac{1}{\gamma}\frac{d\gamma}{d\eta}\right| = \left|\frac{d(\ln\gamma)}{d\eta}\right|$$

From the above derivation, it follows that the parameter B represents the rate at which the pitch angle changes with the shear rate. Since it measures the fractional variation of the pitch angle with respect to the shear rate. Therefore, the parameter B can be interpreted as the decay rate of the pitch angle.

Physically, this quantity describes how rapidly the spiral arms become tightly wound as the shear rate increases. In a differentially rotating galactic disc, differential rotation causes the spiral structure to wind progressively with time. As a result, the pitch angle decreases with increasing shear. A larger value of B therefore indicates a stronger dependence of the pitch angle on shear, implying a faster winding of the spiral arms. Conversely, a smaller value of B corresponds to a weaker dependence of the pitch angle on shear. Using the exponential fitting shown in Figure 3.4, the best-fit parameters are obtained as $A = 30.6 \pm 0.53$ and $B = 0.688 \pm 0.029$ for the case $Q = 1.1$, $\beta = 0.1$, and $X = 1.0$. The fitted curve reproduces the numerical data very well, confirming that the variation of pitch angle with shear rate can be described by an exponential decay relation. The parameter B therefore quantifies the decay rate of the pitch angle with increasing shear for the chosen disc parameters.
This formulation allows us to systematically study how the decay rate of the pitch angle depends on other physical parameters of the disc, such as the Toomre stability parameter Q, the disc scale height parameter β, and the wavelength parameter X. In the following section, we examine how this decay rate varies with β for different values of Q and X.

We examine the variation of decay rate of pitch angle with disc thickness β with different value of Toomre stability factor Q. The main findings are

- The decay rate of the pitch angle exhibits a strong dependence on the disc thickness β for lower values of the Toomre stability parameter Q.
- The decay rate of pitch angle exhibits no dependence on the disc thickness β for higher values of Toomre stability parameter Q.

Figure 3.5 shows the variation of the decay rate of the pitch angle with the disc scale height parameter β for different values of the Toomre stability parameter Q at a fixed wavelength parameter $X = 1.0$. The y axis represents the quantity $\left|\frac{1}{\gamma}\frac{d\gamma}{d\eta}\right|$ or B which corresponds to the exponential decay rate of the pitch angle with shear, and quantifies how rapidly the pitch angle changes as the shear. From the figure 3.5 it is evident that the decay rate depends on both the disc scale height parameter β and the Toomre stability parameter Q, For the lower value of the stability parameter ($Q = 1.1$), the decay rate increases noticeably as β increases. This behaviour indicates that when the galactic disc is close to the threshold of gravitational instability, the vertical thickness of the disc has a strong influence on the evolution of spiral perturbations. Increasing β effectively reduces the self–gravity of the disc in the mid-plane, which weakens the amplification

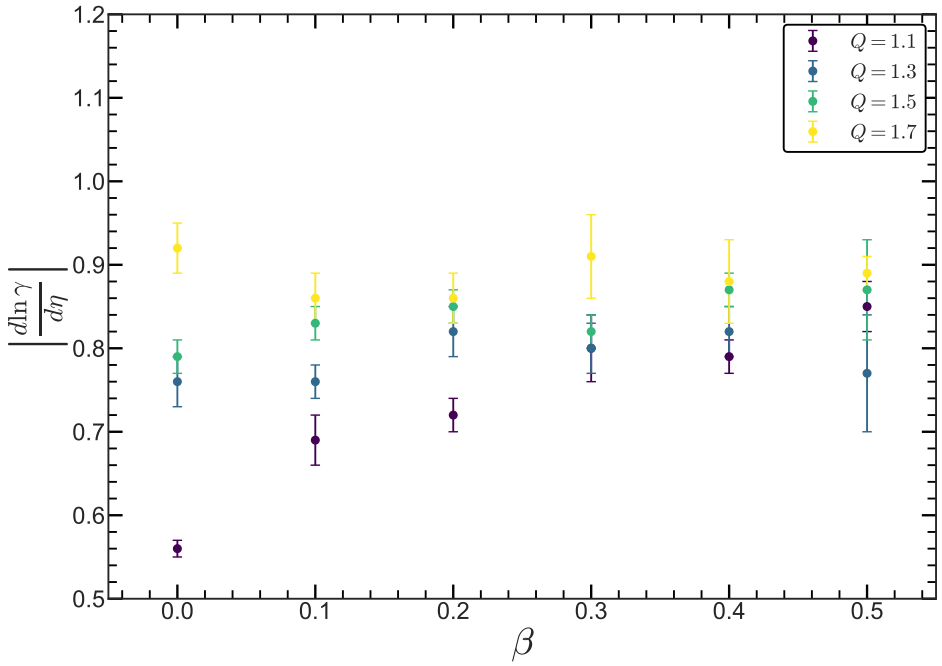


Figure 3.5: *Quantifying the fall-off of the pitch angle with the shear*: the exponential decay rate of the pitch angle with shear, shown for different Toomre Q parameters. For details, see the text.

of perturbations and causes the spiral arms to wind more rapidly under the influence of differential rotation. As a result, the pitch angle decreases more quickly with shear, leading to a larger decay rate.

For higher values of the Toomre parameter ($Q = 1.3, 1.5$, and 1.7), the dependence of the decay rate on β becomes much weaker. In these cases the disc is dynamically hotter and more stable against gravitational perturbations. The stabilizing influence of velocity dispersion already suppresses the growth of spiral structures, and therefore changes in the vertical structure of the disc produce only a modest additional effect. Consequently, the decay rate remains relatively constant across the range of β for larger values of Q.

Another important feature of the figure is that the overall magnitude of the decay rate increases slightly with increasing Q. This suggests that in more stable discs the spiral arms tend to respond more directly to the differential rotation of the galaxy, leading to a more uniform winding behaviour. In contrast, when the disc is close to gravitational instability ($Q \approx 1$), the interplay between self–gravity and shear becomes more complex, causing the decay rate to be more sensitive to variations in disc thickness.

Overall, the results indicate that the vertical structure of the disc plays an important role in regulating the winding of spiral arms, particularly in dynamically cold discs where self–gravity is strong. The effect of disc thickness becomes progressively weaker as the stability of the disc increases, highlighting the dominant role of the Toomre Q parameter in controlling the dynamical response of spiral perturbations.

3.1.3 *Dependence of pitch angle variation with X*

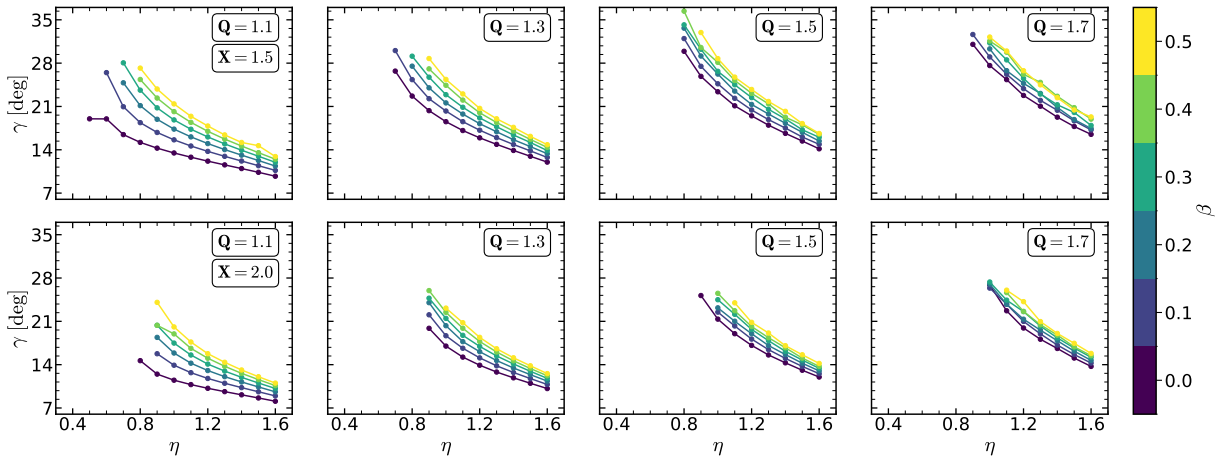


Figure 3.6: Systematic variation of the pitch angle (γ) with the shear rate (η) for swing amplified spiral arms, for different disc scale height (β) and for different value of Toomre Q parameter with different value wavelength parameter 1.5 and 2.0

We examined the variation of pitch angle with shear rate with the inclusion of finite thickness for different value of X. We took the different values of Q (see Figure 3.6) to check the effect of perturbation on stable galactic disc. For a fixed value of the shear parameter η, the pitch angle γ increases systematically with increasing wavelength parameter X. Since larger values of X correspond to perturbations with larger azimuthal wavelength, these perturbations are wound less efficiently by the local shear and therefore retain relatively more open spiral patterns. For both $X = 1.5$ and $X = 2.0$, the pitch angle γ decreases systematically with increasing shear parameter η, indicating that stronger differential rotation produces more tightly wound spiral features. However, for a fixed value of η, the curves corresponding to $X = 2.0$ consistently lie below those for $X = 1.5$. Thus, increasing X leads to smaller values of γ, which corresponds to relatively more closly spiral arms in the standard definition of pitch angle. The wavelength parameter X is defined as $X = \lambda_y/\lambda_{\rm crit}$, where λ_y is the azimuthal wavelength and $\lambda_{\rm crit} = 4\pi^2 G\Sigma/\kappa^2$ is the critical wavelength for gravitational instability. Therefore, larger values of X correspond to perturbations with larger azimuthal wavelength. Since larger-scale perturbations are less susceptible to local shear, they are wound less efficiently as they evolve. Consequently, perturbations with larger X retain relatively more open spiral patterns, leading to lower values of γ.

This trend is also supported by the finite-thickness reduction factor see Eq. 2.20 For larger values of X, the quantity X^{-1} decreases, causing the reduction factor δ to increase. As a result, the suppression of self-gravity due to finite thickness becomes weaker for larger X. Therefore, perturbations with larger azimuthal wavelength experience less damping by finite thickness and can maintain comparatively more open spiral structures. This behavior implies that higher values of X favor the formation of tightly wound spirals. The consistency of this trend across different conditions highlights the strong influence of X on spiral structure. Therefore, X acts as a key parameter governing spiral arm morphology.

3.1.4 *Variation of the pitch angle and shear rate with different values of X*

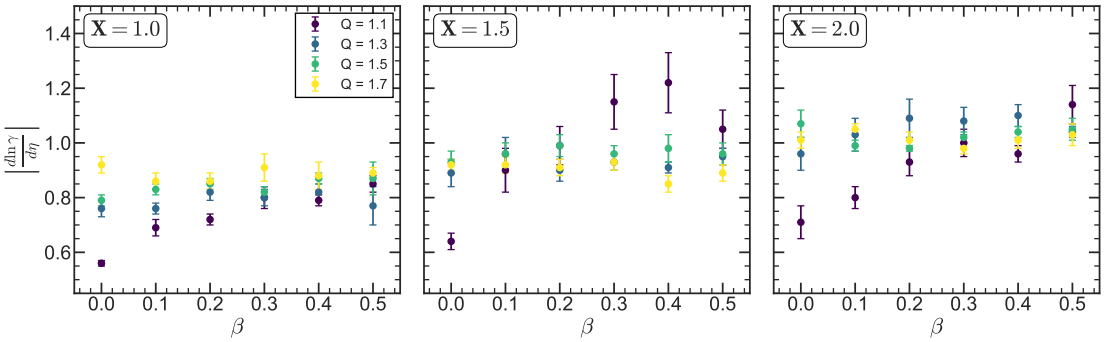


Figure 3.7: *Quantifying the fall-off of the pitch angle with the shear*: the exponential decay rate of the pitch angle with shear, shown for different Toomre Q parameterswith different X values.

We examine the variation of decay rate of pitch angle with disc thickness β with different value of Toomre stability factor Q and X. The main findings are

- The decay rate of the pitch angle exhibits a strong dependence on the disc thickness β for lower values of the Toomre stability parameter Q.
- The decay rate of pitch angle exhibits no dependence on the disc thickness β for higher values of Toomre stability parameter Q

From Figure 3.7, it is evident that the behaviour of the decay rate with increasing disc scale height depends significantly on the stability of the galactic disc Q. For the lowest value of the stability factor ($Q = 1.1$), the decay rate of the pitch angle shows a systematic increase with increasing β. This indicates that thin discs tend to accelerate the decay of the pitch angle when the disc is close to the threshold of gravitational instability.

For larger values of the Toomre stability parameter ($Q = 1.3, 1.5$, and 1.7), the dependence of the decay rate on β becomes much weaker. In these cases, the disc is more stable against gravitational perturbations. As a result, the growth and subsequent decay of spiral features are already strongly regulated by the stabilising Toomre factor. This leads to a nearly almost constant decay rate across the entire range of β for higher values of Q.
A similar qualitative trend is observed for all values of the wavelength parameter X. Although the absolute values of the decay rate vary slightly with X, the overall behaviour remains consistent. In each panel, the decay rate for the lowest Q case shows a clear dependence on β, while the curves corresponding to higher Q values remain relatively flat. This suggests that the influence of disc thickness on the evolution of spiral perturbations is most significant when the disc is close to gravitational instability, whereas its effect becomes less important in more stable systems.
A similar qualitative behaviour is observed for all values of the wavelength parameter X. Although the absolute value of the decay rate changes slightly with X, the overall dependence on the disc thickness parameter β and the Toomre stability parameter Q remains nearly unchanged. This suggests that the wavelength parameter has only a secondary influence on the decay rate of the pitch angle compared to the stronger effects of disc thickness and gravitational stability.

3.2 Comparsion with the past studies

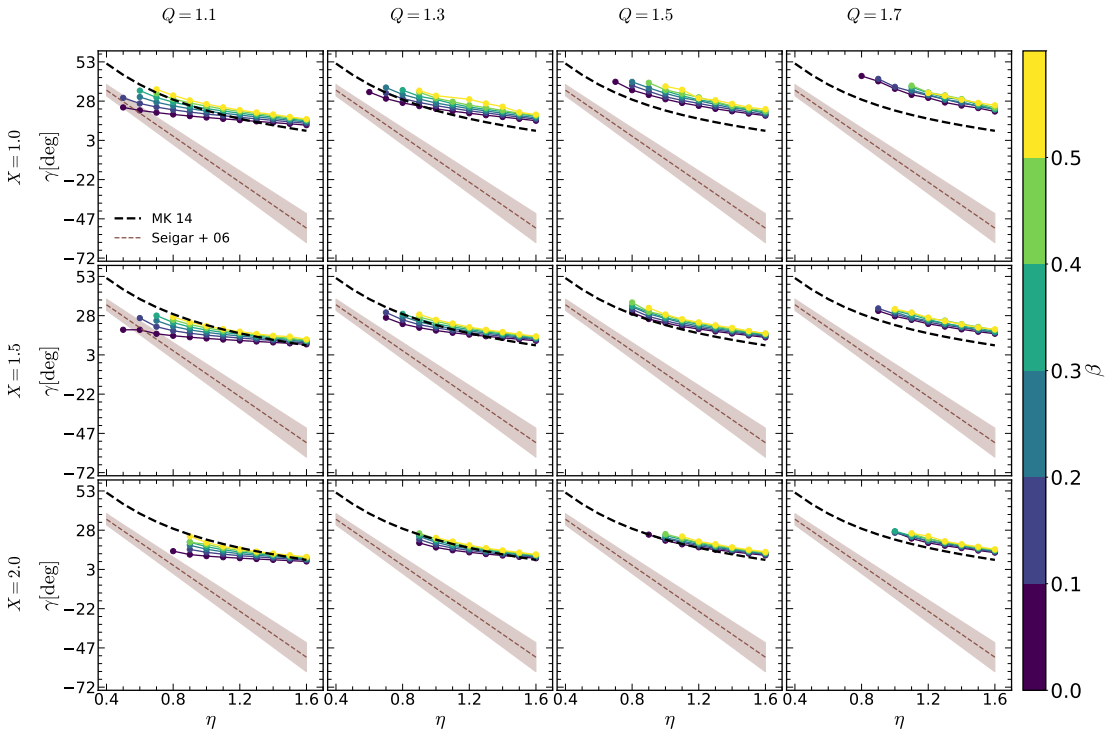


Figure 3.8: Comparison with previous studies: The variation of the pitch angle (γ) with shear rate (η) is shown for different values of the Toomre parameter Q (see columns) and the wavelength parameter X (see rows). The coloured points represent the present calculations from swing amplification for different values of the disc scale height (β), (see the colour bar). The dashed black and grey lines correspond to the best fit results from previous studies Michikoshi and Kokubo (2014) and Marc S. Seigar et al. (2006) respectively. The shaded region represents the observational relation reported in (Marc S. Seigar et al., 2006)

We examined the physical origin of the systematic deviation between the present results and the trends reported in earlier observational and theoretical studies of spiral arm pitch angles. The main findings are

- Although the general trend of decreasing pitch angle with increasing shear rate is consistent with earlier studies, the present results predict systematically different pitch angles than those obtained by Michikoshi and Kokubo (2014) and the observational relation of Marc S. Seigar et al. (2006).

- In swing amplification, the pitch angle depends not only on the shear parameter η but also on additional dynamical parameters such as the Toomre stability parameter Q, the wavelength parameter X, and the finite thickness parameter β. Therefore, the morphology of the resulting spiral arms is determined by the combined effects of shear, self-gravity, pressure, and vertical structure of the disc.

- The discrepancy with earlier studies also partly arises from the different definitions of the shear parameter. In observational studies, the shear parameter is generally derived directly from the measured rotation curve, whereas in the present work it is defined locally in the sheared-frame formalism as $\eta = 2A/\Omega$. Even small

differences in the adopted definition of shear can lead to noticeable differences in the inferred pitch angle.

The results clearly show that all studies consistently predict a systematic decrease in the pitch angle γ with increasing shear rate η. The dashed black curve shown in Figure 3.8 represents the fitting relation obtained by (Michikoshi and Kokubo, 2014). In their work, they investigated the dependence of spiral arm pitch angle on galactic shear using local N–body simulations of collisionless stellar discs. They employed the shearing–box approximation, which allows the local dynamics of a small patch of the galactic disc to be studied in a rotating frame. Their simulations demonstrated that the pitch angle decreases with increasing shear rate, indicating that the winding of spiral arms is primarily controlled by the differential rotation of the galaxy. From their numerical results they derived the empirical relation

$$\tan\gamma = \frac{2}{7}\sqrt{\frac{4-2\eta}{\eta}}, \tag{3.1}$$

which reproduces the trend observed in their simulations. This relation provides a useful theoretical estimate of the spiral arm pitch angle as a function of shear in stellar discs. However, their analysis was restricted to a two–dimensional collisionless stellar system. Important physical effects such as finite disc thickness, gas mass fraction were not included in their simulations. These additional factors can significantly modify the behaviour of spiral density perturbations and therefore influence the resulting pitch angle.

In addition to the simulation results, some observational studies have also explored the relation between spiral arm pitch angle and galactic shear. In particular, (M. S. Seigar et al., 2005; Marc S. Seigar et al., 2006) analysed a sample of nearby grand–design spiral galaxies and reported a strong anti–correlation between pitch angle and shear rate. By measuring the spiral structure using two–dimensional fast Fourier transform (FFT) techniques and combining this information with observed rotation curves, they derived the empirical relation

$$\gamma = (64.25 \pm 2.87) - (73.24 \pm 5.53)\eta. \tag{3.2}$$

This relation indicates that galaxies with larger shear values tend to have smaller pitch angles, confirming the general theoretical expectation that stronger differential rotation produces more tightly wound spiral structure. In their analysis, the shear parameter is determined directly from the observed rotation curve of the galaxy according to

$$\eta_S = \frac{1}{2}\left(1 - \frac{R}{V}\frac{dV}{dR}\right) = \frac{A}{\Omega}, \tag{3.3}$$

This definition depends on the derivative of the rotation curve, the shear parameter reflects the detailed mass distribution of the galaxy and the shape of its rotation profile.

In contrast to the observational definition used by (M. S. Seigar et al., 2005), the present work adopts the theoretical framework of swing amplification in a local sheared galactic disc. In this formalism, the shear parameter is defined as

$$\eta = \frac{2A}{\Omega}, \tag{3.4}$$

as introduced in the classical analysis of (Goldreich and Lynden-Bell, 1965). Although both definitions describe the differential rotation of the galactic disc, they are not numerically identical. The observational definition η_S depends directly on the derivative dV/dR obtained from the measured rotation curve. As a result, even small differences in the definition of the shear parameter can produce noticeable variations in the inferred pitch angle. This difference partly explains why the theoretical results obtained in the present work do not exactly coincide with the observational relation reported by (Marc S. Seigar et al., 2006).

More importantly, the observational relation assumes that the pitch angle is determined primarily by the galactic shear. However, swing amplification theory predicts that the morphology of spiral structure depends on several additional dynamical parameters. One of the most important parameters is the Toomre stability parameter Q, which characterises the stability of the disc against gravitational perturbations. When Q is small, the disc is more susceptible to gravitational instabilities. In this regime, perturbations can grow efficiently through swing amplification, producing strong spiral features with relatively small pitch angles. As the value of Q increases, the disc becomes more stable and the growth of perturbations is suppressed. Consequently, the spiral structure become weaker and more open, leading to larger pitch angles.

Another important factor included in the present framework of swing amplification is the finite thickness of the galactic disc, which is characterized by the parameter β. The inclusion of finite disc thickness modifies the effective self–gravity of the disc.

The comparison presented in Figure 3.8 therefore highlights an important point. While the general trend of decreasing pitch angle with increasing shear is consistent with both numerical simulations and observations, the detailed values of the pitch angle depend on additional physical parameters that are not included in simple empirical relations. his suggests that the swing amplification mechanism provides a more complete realistic description of spiral structure formation, where the morphology of the spiral pattern arises from the complex interplay between shear, self–gravity, epicyclic motion, pressure forces, and disc thickness.

3.3 Variation of swing-amplifies spirals with shear rate for two fluid (stars+gas) case

Galactic discs are multi-component systems composed of stars and interstellar gas, each characterized by distinct dynamical parameter (velocity dispersion). The stellar component behaves as a collisionless system behave as dynamically hotter (high velocity dispersion), whereas the gaseous component and dynamically colder (less velocity dispersion). As a result, the interaction between these two fluids plays a crucial role in determining the stability and evolution of spiral structures. In this section, we investigate the dynamics of a two-fluid disc and examine how the combined effects of stellar and gaseous components alter the swing amplification mechanism and the resulting spiral arm morphology.

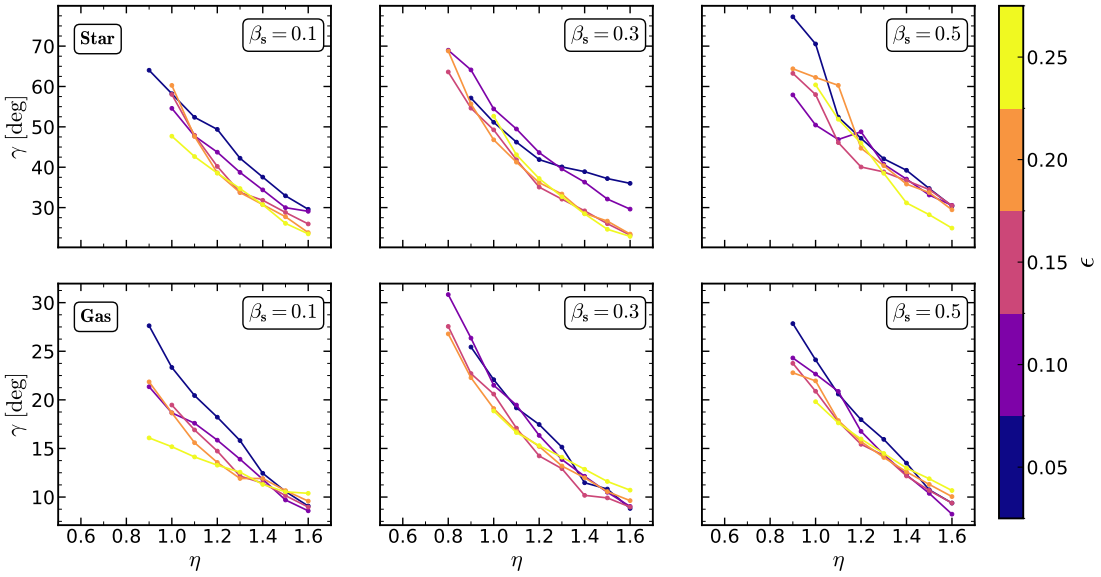


Figure 3.9: Variation of pitch angle (γ) with shear rate (η) for different values of the gas mass fraction (ϵ). The top row corresponds to the stellar component, while the bottom row represents the gaseous component. Each panel shows results for a fixed β_s. Different colored curves denote different values gas mass fraction ϵ, (see the colour bar) while the gas scale height is kept fixed ($\beta_g = 0.1$). In all cases, the pitch angle decreases with increasing shear rate, indicating more tightly wound spiral structures at higher differential rotation.

We examined the variation of pitch angle with shear rate with the inclusion of vary thickness of stellar component ($\beta_s = 0.1, 0.3, 0.5$) and constant thickness of gas component ($\beta_g = 0.1$) for two fluid case with Toomre stability factor $Q_s = 2.0$ & $Q_g = 2.0$. We took the different values of ϵ (see the colour bar) to check the effect of perturbation on stable galactic disc. The gaseous component consistently exhibits smaller pitch angles than the stellar component, indicating that the gas spiral arms are more tightly wound. Furthermore, for both the stellar and gaseous components, the pitch angle decreases with increasing gas mass fraction ϵ, implying that a larger gas content promotes the formation of more tightly bound spiral structures.

Figure 3.9 represents the variation of pitch angle as a function of shear rate for two-fluid galactic disc. In this analysis, both components are characterized by identical Toomre stability parameters, $Q_s = Q_g = 2.0$, which correspondes to a stable galactic disc. The gas scale height is kept fixed at $\beta_g = 0.1$ throughout, allowing a controlled comparison of the influence of stellar thickness on the overall spiral morphology. The pitch angle decreases monotonically with increasing shear rate η for both stellar and gaseous components. At low values of η, the shear is weak, allowing perturbations to grow more freely under the influence of self-gravity, resulting in loosely wound spiral arms characterized by larger pitch angles. As η increases, the stronger differential rotation stretches and shears the perturbations more efficiently, leading to tightly wound spiral structures with smaller pitch angles. This trend is fully consistent with swing amplification for one fluid case, where shear acts as a key parameter controlling the amplification and winding of non-axisymmetric perturbations. Pitch angle is also influenced by galactic disc height. For a given value of η, increasing the stellar disc scale height β_s and β_g systematically results in larger pitch angles. This indicates that thicker stellar discs tend to support more open, loosely wound spiral structures. Physically, this can be understood in terms of the vertical effect of self-gravity: as the disc becomes

thicker, the gravitational force in the mid-plane weakens, reducing the efficiency of swing amplification. The gaseous component generally exhibits smaller pitch angles compared to the stellar component for the same values of η and β_s. This difference can be attributed to the dynamically colder nature of the gas. Gas typically has a lower velocity dispersion compared to stars, making it more responsive to gravitational perturbations and shear. As a result, gas is more efficiently sheared, leading to tighter spiral patterns. In contrast, the stellar component, being dynamically hotter, resists swing amplification and forms relatively more open spiral structures. As gas mass fraction ϵ increases, there is a systematic reduction in the overall pitch angle for both components. This suggests that higher values of ϵ act to suppress the formation of loosely wound structures and instead favor tighter spiral patterns. In a physical sense, this indicates that ϵ influences the balance between self-gravity and shear, effectively modifying the efficiency of swing amplification. At larger ϵ, the amplification of perturbations becomes less efficient, and the dominant effect of shear leads to more tightly wound spirals.

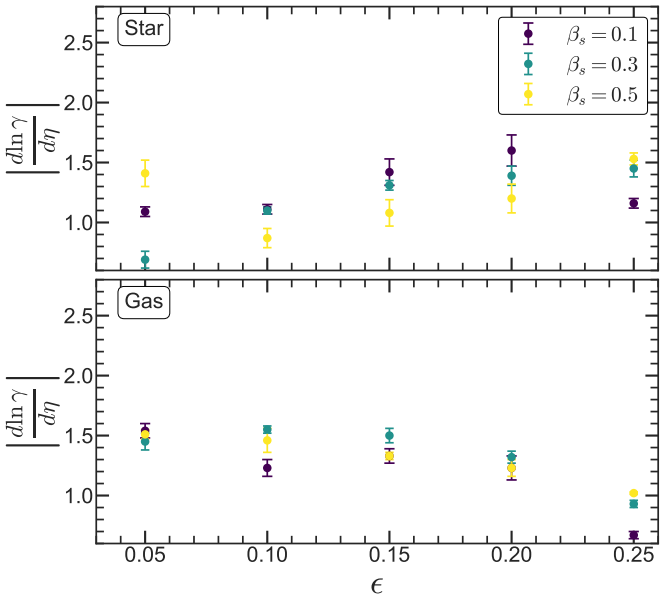


Figure 3.10: The exponential decay of pitch angle with shear rate for two fluid case, shown for different value of gas mass fraction (ϵ), with different value of disc scale height and Toomre factor ($Q_s = 2.0, Q_g = 2.0$)**.**

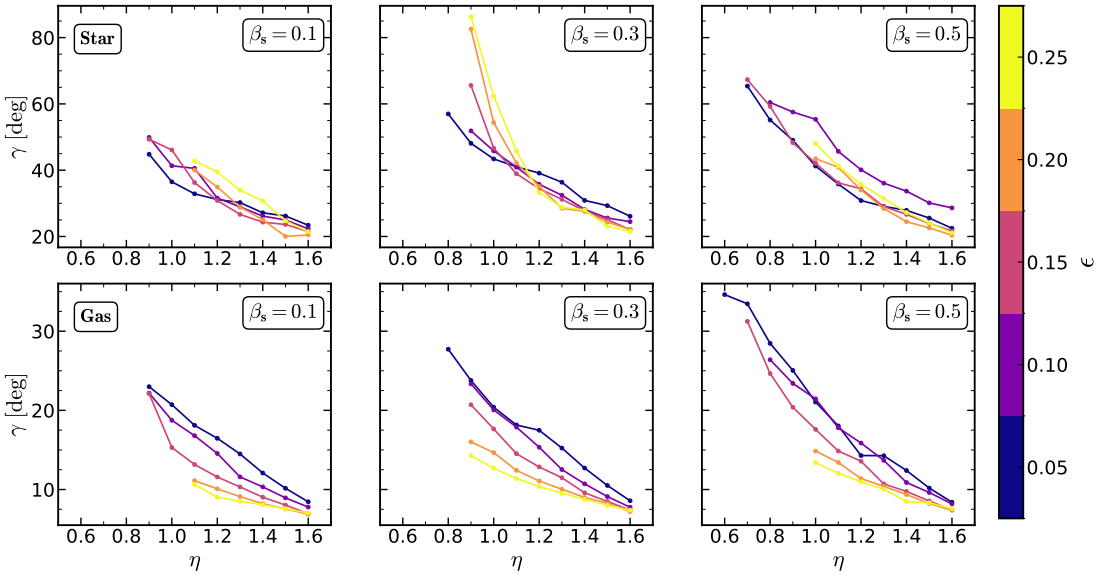


Figure 3.11: Variation of pitch angle (γ) with shear rate (η) for different values of the gas mass fraction ϵ. The top row corresponds to the stellar component, while the bottom row represents the gaseous component. Each subplot shows results for a fixed β_s and β_g. Different colored curves denote different values of gas mass fraction ϵ, while the gas scale height is kept fixed ($\beta_g = 0.1$). In all cases, the pitch angle decreases with increasing shear rate, indicating more tightly wound spiral structures at higher differential rotation.

We examined the variation of pitch angle with shear rate with the inclusion of vary thickness of stellar component ($\beta_s = 0.1, 0.3, 0.5$) and constant thickness of gas component ($\beta_g = 0.1$) for two fluid case with Toomre stability factor ($Q_s = 1.8, Q_g = 1.2$). We took the different values of ϵ (see the colour bar) to check the effect of perturbation on stable galactic disc. The gaseous component consistently exhibits smaller pitch angles than the stellar component, indicating that the gas spiral arms are more tightly wound. Furthermore, for both the stellar and gaseous components, the pitch angle decreases with increasing gas mass fraction ϵ, implying that a larger gas content promotes the formation of more tightly bound spiral structures.

Figure 3.11 represent the variation of pitch angle as a function of shear rate for two-fluid galactic disc. In this analysis, both components are characterized by different Toomre stability parameters, $Q_s = 1.8, Q_g = 1.2$, which correspondes to a stable galactic disc. The gas scale height is kept fixed at $\beta_g = 0.1$ throughout, allowing a controlled comparison of the influence of stellar thickness on the overall spiral morphology. The pitch angle decreases monotonically with increasing shear rate η for both stellar and gaseous components. At low values of η, the shear is weak, allowing perturbations to grow more freely under the influence of self-gravity, resulting in loosely wound spiral arms characterized by larger pitch angles. As η increases, the stronger differential rotation stretches and shears the perturbations more efficiently, leading to tightly wound spiral structures with smaller pitch angles. This trend is fully consistent with swing amplification for one fluid case, where shear acts as a key parameter controlling the amplification and winding of non-axisymmetric perturbations. Pitch angle is also influenced by galactic disc height. For a given value of η, increasing the stellar disc scale height β_s and β_g systematically results in larger pitch angles. This indicates that thicker stellar discs tend to support more open, loosely wound spiral structures. Physically, this can be understood in terms of the vertical effect of self-gravity: as the disc becomes

thicker, the gravitational force in the mid-plane weakens, reducing the efficiency of swing amplification. The gaseous component generally exhibits smaller pitch angles compared to the stellar component for the same values of η and β_s. This difference can be attributed to the dynamically colder nature of the gas. Gas typically has a lower velocity dispersion compared to stars, making it more responsive to gravitational perturbations and shear. As a result, gas is more efficiently sheared, leading to tighter spiral patterns. In contrast, the stellar component, being dynamically hotter, resists swing amplification and forms relatively more open spiral structures. As gas mass fraction ϵ increases, there is a systematic reduction in the overall pitch angle for both components. This suggests that higher values of ϵ act to suppress the formation of loosely wound structures and instead favor tighter spiral patterns. In a physical sense, this indicates that ϵ influences the balance between self-gravity and shear, effectively modifying the efficiency of swing amplification. At larger ϵ, the amplification of perturbations becomes less efficient, and the dominant effect of shear leads to more tightly wound spirals.

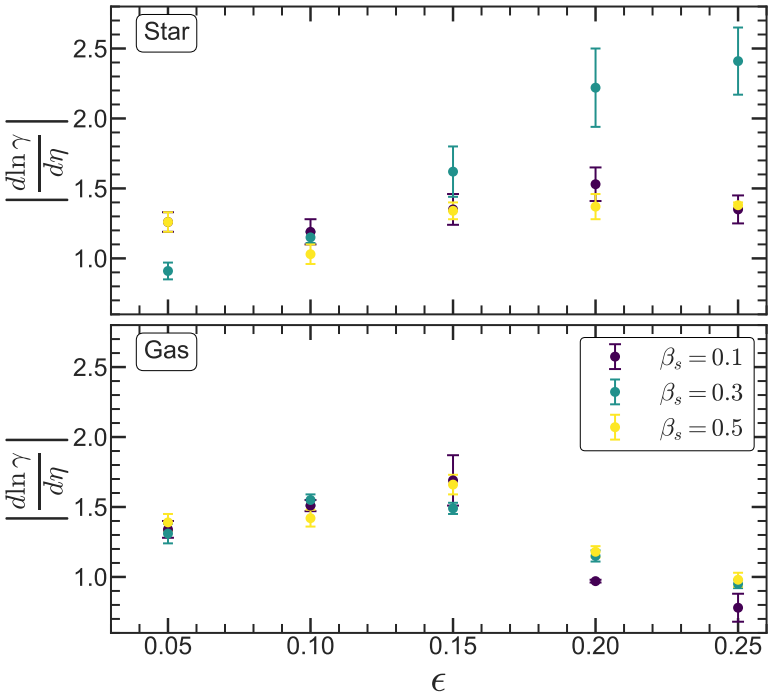


Figure 3.12: The exponential decay of pitch angle with shear rate for the two-fluid case, shown for different values of gas mass fraction (ϵ) and disc scale height, with ($Q_s = 1.8, Q_g = 1.2$)

Chapter 4

Conclusion & Future Plans

In summary, we have studied the dynamical effect of disc shear, disc thickness, and interstellar gas on pitch angle of swing amplified spirals in galaxies. This was done by modelling the galactic disc first as a one-fluid (stars) and then as a gravitationally-coupled two-fluid (stars + gas) system. The main results obtained from this work are summarized below.

The present analysis shows that the pitch angle of swing-amplified spiral structure decreases systematically with increasing shear rate for all explored values of the Toomre stability parameter Q and wavelength parameter X, indicating that stronger differential rotation produces more tightly wound spirals. Finite disc thickness increases the pitch angle, leading to relatively more open spiral structure than in infinitesimally thin discs, while simultaneously reducing the maximum amplification factor (MAF) by weakening the self-gravity of the perturbation. The Toomre stability parameter Q strongly regulates both the morphology and strength of spiral structure: larger values of Q suppress the MAF and produce more open spiral arms, reflecting the increasing dynamical stability of the disc. Similarly, increasing the wavelength parameter X decreases both the pitch angle and the MAF, implying that larger-scale perturbations are less efficiently amplified and tend to form tighter spirals. The relation between pitch angle and shear rate is well described by an exponential decay law, with the decay rate depending on Q, X, and the finite thickness parameter β. However, at sufficiently large values of Q, the decay rate becomes nearly independent of disc thickness. In the gravitationally coupled (stars and gas) system, the overall trend of decreasing pitch angle with increasing shear remains unchanged, although increasing the gas fraction produces tighter spiral arms because the gaseous component is dynamically colder and responds more strongly to non-axisymmetric perturbations. Overall, these results demonstrate that spiral arm morphology is governed by the combined effects of shear, self-gravity, disc stability, finite thickness, and gas content.

Based on the finding, as per presented here, I wish to carry out the following research ideas in the future. An important open question in extragalactic astronomy is how the morphology of spiral arms evolves across cosmic time. Observations of disc galaxies at redshifts $z \sim 1$–2 reveal that these systems have significantly higher gas mass fractions ($\epsilon \sim 0.3$–0.5) and higher levels of interstellar turbulence compared to their local counterparts, with typical gas fractions in the local Universe of $\epsilon \sim 0.05$–0.15. The Toomre parameter Q also evolves with redshift, as the interplay between gas accretion, star formation, and feedback processes modifies the stability of the disc over cosmic time. The present work demonstrates that increasing the gas mass fraction ϵ systematically decreases the pitch angle of both the stellar and gaseous spiral arms, while decreasing Q increases the strength of swing amplification and drives more tightly wound spiral patterns. These results imply that high-redshift disc galaxies, which have higher ϵ and lower effective Q, are expected to host more tightly wound spiral arms than local disc galaxies at the same shear rate. By combining the pitch angle–shear relation derived in the present work with observational and theoretical constraints on the redshift evolution of $\epsilon(z)$ and $Q(z)$ from cosmological simulations and galaxy surveys, it is possible to predict how the pitch angle distribution of spiral galaxies evolves between

$z \sim 2$ and $z = 0$. Such predictions can now be tested directly with observations from the James Webb Space Telescope (JWST), which is beginning to resolve the internal structure of disc galaxies at $z \gtrsim 1$ with unprecedented sensitivity and angular resolution. In particular, JWST rest-frame optical and near-infrared imaging of spiral galaxies at $z \sim 1$–2 provides a direct measure of the pitch angle in the old stellar disc, which can be compared with the predictions of the swing amplification model at the appropriate redshift-dependent values of ϵ and Q. This would open an entirely new observational window on the dynamical evolution of galactic disc structure across cosmic time and would represent a significant extension of the theoretical framework developed in the present thesis.

REFERENCES

Athanassoula, Evangélie (1984). "The spiral structure of galaxies". In: *Physics Reports* 114.5-6, pp. 319–403.

Baba, J., T. R. Saitoh, and K. Wada (2013). "The Dynamics of Transient and Recurrent Spiral Arms in Disk Galaxies". In: *The Astrophysical Journal* 763, p. 46.

Bertin, G. and C. C. Lin (1996). *Spiral Structure in Galaxies: A Density Wave Theory*. Cambridge, MA: MIT Press.

Binney, J. and S. Tremaine (2008). *Galactic Dynamics*. 2nd. Princeton University Press.

Buta, Ronald (Jan. 1989). "Galaxy morphology and classification." In: *World of Galaxies (Le Monde des Galaxies)*. Ed. by Harold G. Corwin Jr. and Lucette Bottinelli, pp. 29–44.

Calzetti, D. et al. (2007). "The Calibration of Monochromatic Far-Infrared Star Formation Rate Indicators". In: *The Astrophysical Journal* 666.2, pp. 870–895. DOI: 10.1086/520082.

Chandar, R. et al. (2016). "The Star Cluster Age Distribution Across Spiral Arms". In: *The Astrophysical Journal* 824, p. 71.

D'Onghia, Elena, Mark Vogelsberger, and Lars Hernquist (2013). "Self-perpetuating spiral arms in disk galaxies". In: *The Astrophysical Journal* 766.1, p. 34.

Dobbs, C. and J. Baba (2014). "Spiral Structures in Disk Galaxies". In: *Publications of the Astronomical Society of Australia* 31, e035.

Dobbs, C. L. and J. Baba (2014). "Spiral Structures in Disk Galaxies". In: *Publications of the Astronomical Society of Australia* 31, e035.

Dobbs, C. L. and J. E. Pringle (2010). "The exciting lives of spiral arms". In: *Monthly Notices of the Royal Astronomical Society* 409, pp. 396–404.

Dobbs, C. L., C. Theis, et al. (2013). "Gas Dynamics and Star Formation in Spiral Galaxies". In: *Monthly Notices of the Royal Astronomical Society* 430, pp. 1538–1544.

Elmegreen, B. G. (1995). "An effective Q parameter for two-fluid instabilities in spiral galaxies". In: *Monthly Notices of the Royal Astronomical Society* 275.4, pp. 944–950. DOI: 10.1093/mnras/275.4.944.

Elmegreen, D. M. and B. G. Elmegreen (1982). "Flocculent and grand design spiral structure in galaxies". In: *The Astrophysical Journal* 386, pp. 295–307.

— (1987). "Arm Classifications for Spiral Galaxies". In: *The Astrophysical Journal* 314, pp. 3–. DOI: 10.1086/165034.

Elmegreen, DEBRA MELOY and BRUCE G Elmegreen (1984). "Blue and near-infrared surface photometry of spiral structure in 34 nonbarred grand design and flocculent galaxies". In: *Astrophysical Journal Supplement Series (ISSN 0067-0049), vol. 54, Jan. 1984, p. 127-149.* 54, pp. 127–149.

Elmegreen, Debra Meloy and Bruce G Elmegreen (2013). "The onset of spiral structure in the universe". In: *The Astrophysical Journal* 781.1, p. 11.

Fabbiano, G. (1989). "X Rays from Normal Galaxies". In: *Annual Review of Astronomy and Astrophysics* 27, pp. 87–138. DOI: 10.1146/annurev.aa.27.090189.000511.

Foyle, K., H.-W. Rix, C. L. Dobbs, A. Leroy, et al. (2011). "Star Formation and Gas Motions in Spiral Galaxies". In: *The Astrophysical Journal* 735, p. 101.

Foyle, K., H.-W. Rix, C. L. Dobbs, A. K. Leroy, et al. (2011). "Star Formation and the Spiral Structure of Nearby Galaxies". In: *The Astrophysical Journal* 735.2, p. 101. DOI: 10.1088/0004-637X/735/2/101.

Fuchs, Burkhard (2001). "Density waves in the shearing sheet-I. Swing amplification". In: *Astronomy & Astrophysics* 368.1, pp. 107–121.

Ghosh, Soumavo and Chanda J Jog (2014). "Suppression of gravitational instabilities by dominant dark matter halo in low-surface-brightness galaxies". In: *Monthly Notices of the Royal Astronomical Society* 439.1, pp. 929–935.

— (2018). "Dwarf irregular galaxies with extended HI gas disks: Suppression of small-scale spiral structure by dark matter halo". In: *New Astronomy* 63, pp. 38–47.

Goldreich, Peter and D Lynden-Bell (1965). "II. Spiral arms as sheared gravitational instabilities". In: *Monthly Notices of the Royal Astronomical Society* 130.2, pp. 125–158.

Grand, R. J. J., D. Kawata, and M. Cropper (May 2013). "Spiral arm pitch angle and galactic shear rate in N-body simulations of disc galaxies". In: 553, A77, A77. DOI: 10.1051/0004-6361/201321308. arXiv: 1209.4083 [astro-ph.GA].

Hodge, J. A. et al. (2019). "Resolved Structure of High-Redshift Galaxies". In: *The Astrophysical Journal* 876, p. 130.

Jog, Chanda J and PM Solomon (1984). "Two-fluid gravitational instabilities in a galactic disk". In: *The Astrophysical Journal* 276, pp. 114–126.

Jog, Chanda J. (May 1992). "Swing Amplification of Nonaxisymmetric Perturbations in Stars and Gas in a Sheared Galactic Disk". In: *The Astrophysical Journel* 390, p. 378. DOI: 10.1086/171289.

— (May 2014). "title = Effective Q Criterion for Disk Stability in an External Potential," in: *The Astronomical Journal* 147.6, p. 132. DOI: 10.1088/0004-6256/147/6/132. URL: https://doi.org/10.1088/0004-6256/147/6/132.

Julian, W. H. and A. Toomre (1966). "Non-Axisymmetric Responses of Differentially Rotating Disks". In: *The Astrophysical Journal* 146, p. 810.

Kennicutt, R. C. (1998). "Star Formation in Galaxies Along the Hubble Sequence". In: *Annual Review of Astronomy and Astrophysics* 36, pp. 189–231. DOI: 10.1146/annurev.astro.36.1.189.

Kormendy, John and Robert C. Kennicutt (2004). "Secular Evolution and the Formation of Pseudobulges in Disk Galaxies". In: *Annual Review of Astronomy and Astrophysics* 42, pp. 603–683. DOI: 10.1146/annurev.astro.42.053102.134024.

Kreckel, K., G. A. Blanc, E. Schinnerer, et al. (2016). "An Optical View of Star Formation Relative to Spiral Arms". In: *The Astrophysical Journal* 827, p. 103.

Lin, C. C. and Frank H. Shu (1964a). "On the Spiral Structure of Disk Galaxies". In: *The Astrophysical Journal* 140, p. 646.

— (Aug. 1964b). "On the Spiral Structure of Disk Galaxies." In: *The Astrophysical Journel* 140, p. 646. DOI: 10.1086/147955.

Meidt, S. E. et al. (2013). "Revealing the Stellar Mass Distribution in Spiral Galaxies". In: *The Astrophysical Journal* 779.1, p. 45. DOI: 10.1088/0004-637X/779/1/45.

Merrifield, M. R. and R. Kurosawa (2000). "Determining Pattern Speeds in Spiral Galaxies". In: *Monthly Notices of the Royal Astronomical Society* 313, pp. 995–1004.

Michikoshi, Shugo and Eiichiro Kokubo (May 2014). "title = Pitch Angle of Galactic Spiral Arms," in: *The Astrophysical Journal* 787.2, p. 174. DOI: 10.1088/0004-637X/787/2/174. URL: https://doi.org/10.1088/0004-637X/787/2/174.

— (2016). “Swing Amplification of Galactic Spiral Arms: Phase Synchronization of Stellar Epicycle Motion”. In: *The Astrophysical Journal* 823.2, p. 121.
NASA Goddard Space Flight Center (2010). *The Milky Way in Multiple Wavelengths*. https://asd.gsfc.nasa.gov/archive/mwmw/mmw_images.html. Multi-wavelength composite images of the Milky Way from radio to gamma rays.
Oh, S. H. et al. (2015). “Tidal Origin of Spiral Arms in Disk Galaxies”. In: *The Astrophysical Journal* 807, p. 73.
Savchenko, Sergey et al. (2020). “A multiwavelength study of spiral structure in galaxies. I. General characteristics in the optical”. In: *Monthly Notices of the Royal Astronomical Society* 493.1, pp. 390–409.
Schinnerer, E. et al. (2017). “The Anatomy of Star Formation in Nearby Spiral Galaxies”. In: *Astrophysical Journal* 836, p. 62.
Seigar, M. S. et al. (May 2005). “Dust-penetrated arm classes: insights from rising and falling rotation curves”. In: *Monthly Notices of the Royal Astronomical Society* 359.3, pp. 1065–1076. ISSN: 0035-8711. DOI: 10.1111/j.1365-2966.2005.08970.x. eprint: https://academic.oup.com/mnras/article-pdf/359/3/1065/2896627/359-3-1065.pdf. URL: https://doi.org/10.1111/j.1365-2966.2005.08970.x.
Seigar, Marc S. et al. (July 2006). “Constraining Dark Matter Halo Profiles and Galaxy Formation Models Using Spiral Arm Morphology. I. Method Outline”. In: *The Astrophysical Journal* 645.2, p. 1012. DOI: 10.1086/504463. URL: https://doi.org/10.1086/504463.
Sellwood, J. A. (2011). “Transient spiral structure in disk galaxies”. In: *Monthly Notices of the Royal Astronomical Society* 410, pp. 1637–1646.
— (2014). “A review of spiral structure in disk galaxies”. In: *Reviews of Modern Physics* 86.1, pp. 1–46.
Sellwood, J. A. and R. G. Carlberg (1984). “Spiral instabilities provoked by accretion and star formation”. In: *The Astrophysical Journal* 282, p. 61.
Sellwood, J. A. and L. S. Sparke (1988). “Bar-driven Spiral Structure”. In: *Monthly Notices of the Royal Astronomical Society* 231, pp. 25–52.
Shabani, F. et al. (2018). “Testing Spiral Arm Formation Mechanisms Through Age Gradients”. In: *Monthly Notices of the Royal Astronomical Society* 478, p. 3590.
Shu, Frank H (2016). “Six decades of spiral density wave theory”. In: *Annual Review of Astronomy and Astrophysics* 54.1, pp. 667–724.
Strickland, D. K. et al. (2004). “A High Spatial Resolution X-Ray and Hα Study of Hot Gas in the Halos of Star-forming Disk Galaxies. II. Quantifying Supernova Feedback”. In: *The Astrophysical Journal Supplement Series* 151.1, pp. 193–236. DOI: 10.1086/382214.
Tamburro, D. et al. (2008). “What Sets the Star Formation Timescale in Galaxies?” In: *The Astronomical Journal* 136.6, pp. 2872–2884. DOI: 10.1088/0004-6256/136/6/2872.
Toomre, A. (May 1964). “On the gravitational stability of a disk of stars.” In: *The Astrophysical Journel* 139, pp. 1217–1238. DOI: 10.1086/147861.
— (Jan. 1981). “What amplifies the spirals”. In: *Structure and Evolution of Normal Galaxies*. Ed. by S. M. Fall and D. Lynden-Bell, pp. 111–136.
Willett, K. W. et al. (2017). “Galaxy Zoo: Bar and Spiral Arm Evolution”. In: *Monthly Notices of the Royal Astronomical Society* 464, pp. 4176–4190.

Yu, Si-Yue et al. (July 2018). “The Carnegie-Irvine Galaxy Survey. VI. Quantifying Spiral Structure”. In: *The Astrophysical Journal* 862.1, p. 13. DOI: 10.3847/1538-4357/aacb25. URL: https://doi.org/10.3847/1538-4357/aacb25.